Chemical Engineering Science 262 (2022) 117925

Contents lists available at ScienceDirect

Chemical Engineering Science

journal homepage: www.elsevier.com/locate/ces

A conservative finite volume method for the population balance equation with aggregation, fragmentation, nucleation and growth

Daniel O'Sullivan, Stelios Rigopoulos *

Department of Mechanical Engineering, Imperial College London, South Kensington Campus, London SW7 2AZ, UK

HIGHLIGHTS

- Discretisation method for the population balance is developed.
- Method is mass conservative, applicable to arbitrary grid, efficient and accurate.
- Applicable to any combination of aggregation, fragmentation, nucleation and growth.
- Method is tested with reference solutions.
- Very accurate results are obtained for both distribution and moments.

ARTICLE INFO

Article history:
Received 30 March 2022
Received in revised form 11 July 2022
Accepted 15 July 2022
Available online 30 July 2022

Keywords:
Population balance
Aggregation
Fragmentation
Growth
Numerical solution
Finite volume method

ABSTRACT

In the present paper, we present a method for solving the population balance equation (PBE) with the complete range of kinetic processes included: namely aggregation, fragmentation, nucleation and growth. The method is based on the finite volume scheme and features guaranteed conservation of the first moment by construction, accurate prediction of the size distribution, applicability to an arbitrary non-uniform grid, robustness and computational efficiency which is instrumental for coupling with computational fluid dynamics (CFD). The treatment of aggregation is based on the previous work by Liu and Rigopoulos (2019). An analysis of the aggregation terms in the PBE is made, and the source of conservation error in finite element/volume methods is elucidated. It is subsequently shown how this error is overcome in the present method via a coordinate transformation applied to the aggregation birth double integral resulting from the application of the finite volume method. The contributions to the birth term are delineated and their corresponding death fluxes identified. An aggregation map is then constructed for mapping birth and death fluxes, thus allowing the finite volume method to operate in terms of fluxes and achieve conservation of mass. The method is then extended to fragmentation, for which a map is also constructed to represent the birth and death fluxes. In the implementation, the aggregation and fragmentation maps are pre-tabulated to allow fast computation. It is also shown how the method can be coupled with a total variation diminishing (TVD) scheme for the treatment of growth with minimal numerical diffusion. The method is validated with a number of test cases including analytical solutions and numerical solutions of the discrete PBE for aggregation (theoretical and free molecule/Brownian kernels), fragmentation, aggregation-fragmentation and aggregation-growth. In all cases, the method produces very accurate results, while also being computationally efficient due to the pre-tabulation of the maps and the simplicity of the algorithm carried out per time step.

1. Introduction

The Population Balance Equation (PBE) governs a wide range of problems featuring a population of entities with a distribution of one or more properties. Examples include particulate processes, aerosols, colloids, polymers and biochemical problems. The earliest form of the PBE is a discrete equation proposed by Smoluchowski (1917) to describe the coagulation of colloidal particles. Since then, the scope of that formulation has been expanded by several authors to a more general and continuous equation that accounts for a range of kinetic processes, namely aggregation, fragmentation, nucleation, growth, as well as transport in physical space. Reviews of the general aspects of the PBE can be found in

* Corresponding author.
E-mail address: s.rigopoulos@imperial.ac.uk (S. Rigopoulos).

https://doi.org/10.1016/j.ces.2022.117925
0009-2509/

Ramkrishna (1985, 1998, 2000, 2002, 2014, 2012, 2015), among others. There are also more specific reviews focussing on particular processes and applications such as: Kostoglou et al. (2007) for breakage processes, Williams and Loyalka (1991) for aerosols, and Rigopoulos (2019) for soot formation. Reviews focussed on solution methods are (Drake et al., 1972; Williams and Loyalka, 1991; Kumar et al., 2007), and reviews aimed at the coupling of PBE with fluid dynamics are (Rigopoulos, 2010; Raman and Fox, 2016; Shiea et al., 2020). It should also be mentioned that various forms of the PBE have appeared under different names, such as Smoluchowski equation or General Dynamic Equation (GDE).

The PBE for a spatially homogeneous system is shown below:

$$\begin{aligned}\frac{\partial n(v,t)}{\partial t}+\frac{\partial (G(v)n(v,t))}{\partial v} &= B\delta(v-v_{nuc})\\ +\frac{1}{2}\int_0^v \beta(w,v-w)n(w,t)n(v-w,t)dw&\\ -n(v,t)\int_0^\infty \beta(v,w)n(w,t)dw&\\ +\int_v^\infty \gamma(w)p(v,w)n(w,t)dw-\gamma(v)n(v,t)&\end{aligned} \tag{1}$$

where $n(v,t)$ is the number density of particles with volume between v and $v+dv$, and is also known as the particle size distribution, $G(v)$ is the growth rate, B is the nucleation rate, v_{nuc} is the size of the nuclei, $\beta(v,w)$ is the aggregation kernel (rate of aggregation events), $\gamma(v)$ is the fragmentation kernel (rate of fragmentation events) and $p(v,w)$ is the fragment size distribution or daughter size distribution. The formulation in terms of particle volume (or equivalently mass for constant density particles) is advantageous for problems involving aggregation and fragmentation, as particle volume is conserved throughout these processes. The equation can be extended to multiple dimensions, when more than one distributed property among particles is involved. Furthermore, in problems involving fluid flows, spatial transport terms accounting for convective and diffusive transport can be included. This leads to the coupling of the PBE with the flow field.

The solution of the continuous PBE in its most general form is a difficult problem to which a considerable volume of literature has been devoted. The difficulty arises partly from the need to accommodate several processes with different characteristic features. For example, aggregation and fragmentation processes give rise to integro-differential equations, while growth endows the PBE with the nature of a hyperbolic partial differential equation. Very few analytical solutions have been found, and apply only to special cases. Numerical methods are thus required for solving the PBE in practical problems. The main classes of solution methods employed in practice are Monte Carlo, moment and discretisation methods. Monte Carlo methods for the PBE date from the work of Spielman and Levenspiel (1965) and a review of early works can be found in Ramkrishna (2000). They are computationally expensive but able to accommodate multi-dimensional problems without an accompanying exponential increase in computational time. Moment methods, originating in early works such as those of Hulburt and Katz (1964) and Thompson (1968), aim to solve for the moments of the distribution. As such, they represent the most economical method of solution, but do not compute the particle size distribution itself, and require further models as the moment equations are generally unclosed - except for certain special cases. Discretisation methods, of which early examples are the works of Bleck (1970) and Gelbard and Seinfeld (1978), offer prediction of the particle size distribution and do not require closure, but need considerable attention to minimise numerical and conservation errors, and become expensive for high-dimensional problems. Methods have also been proposed that combine concepts of moment and discretisation methods (e.g. Nguyen et al. (2016);Laurent et al. (2016);Yang and Mueller (2019)).

While every one of these categories of methods offers its own advantages and disadvantages that render it more or less suitable for particular purposes, the present work is devoted to discretisation methods. This class of methods has attracted increased interest lately, due to the need to predict the distributions of important properties in a number of problems. For example, the particle size distribution is of utmost importance in atmospheric aerosols, as it determines the health impacts of the aerosol pollutants - ultrafine particles, for instance, can penetrate deep into the lungs. In applications involving the formation of a particulate product such as flame synthesis of nanoparticles and crystallisation, the distribution of size and morphology determines the properties of the product and must be tailored to specific applications. Another emerging issue is the coupling of PBE solution methods with computational fluid dynamics (CFD), which is needed for many problems such as aerosol formation and crystallisation that involve a fluid flow. This coupling requires the solution of a very large number of local PBEs (resulting from the spatial discretisation of the spatially dependent PBE), bringing the efficiency of the method to the fore. Furthermore, several sources of error (CFD solution, PBE solution, physical and chemical models, turbulence-chemistry interaction) may be present in the results, which makes the comparison with experiments very difficult. Highly accurate numerical methods are pivotal for minimising numerical uncertainties and preventing compensation of errors.

The literature on discretisation methods for the PBE includes a large number of works. In order to put the present contribution into context, it is helpful to identify certain groups of methods with common features. The discretisation of the aggregation-fragmentation terms will be discussed first, and three main groups of methods can be identified.

Methods in the first group approximate the distribution as a sum of delta functions, thus replacing the continuous PBE with a discrete equivalent. In the case of a uniform grid, this is equivalent to the discrete PBE but requires an excessive amount of nodes. When a non-uniform grid is employed, most of the daughter particles do not lie on grid nodes and therefore their mass must be distributed among neighbouring nodes using correction factors. This operation is performed such that one or more moments are conserved, and thus methods in this class are conservative (with respect to the particular moments) by construction. However, this procedure results in modifications in the particle size distribution. The earliest method in this category is that of Batterham et al. (1981) and conserves only mass. The method of Hounslow et al. (1988) conserves both number of particles as well as mass, and also accommodates nucleation and growth together with aggregation. The later methods of Litster et al. (1995) and Hill and Ng (1996) allow for a wider range of grids. This concept was further extended by Kumar and Ramkrishna (1996a,b) (the fixed and moving pivot techniques), whose method is applicable to an arbitrary grid. Kumar et al. (2006), further improved the discretised representation of the distribution (the cell average technique), and Kostoglou (2007) extended the cell average technique to the conservation of three moments.

A second group of methods directly discretise the population balance with finite element or finite volume schemes. However, the PBE with aggregation and fragmentation is an integro-differential equation, and therefore the application of such a method results in double integrals. In methods belonging to this class, the inner integrals generated are approximated with one-dimensional quadrature, and the resulting polynomial expression is then integrated again over an element. Therefore, these methods focus on correct prediction of the particle size distribution, but face problems with conservation of moments that can only be miti-

gated by increased accuracy achieved via higher order approximations or finer grids. The origin of the conservation error will be elaborated further in the present paper (cf. Section 2.3), but we briefly mention here that it is associated with the convolution-like aggregation birth term. Methods in this category include the earlier approach of Gelbard and Seinfeld (1978) and the methods of Nicmanis and Hounslow (1998) and Roussos et al. (2005). Rigopoulos and Jones (2003) presented a method of this type that aimed to reduce the conservation error and shares some concepts with the present work.

A third group comprises methods that are also based on the application of the finite volume method to the population balance. The difference with the methods in the second group is that the double integrals are here treated directly with two-dimensional quadrature. This feature allows the methods in the third group to accomplish exact conservation of one moment (typically the first one) without modifying the distribution. The first of such methods was developed by Bleck (1970), and was derived in an ad hoc manner. However, the complexity of dealing with the bounds of the double integrals has limited many such methods to geometric grids. These include, apart from the work of Bleck (1970), the methods of Gelbard et al. (1980,) and Landgrebe and Pratsinis (1990). Filbet and Laurençot (2004) developed a method based on an alternative form of the aggregation equation, and investigated its mathematical properties. Liu and Rigopoulos (2019) developed a conservative finite volume method that is applicable to arbitrary grids and forms the basis for the present work.

Several of the methods mentioned above (Batterham et al., 1981; Kumar and Ramkrishna, 1996a; Kumar and Ramkrishna, 1996b; Nicmanis and Hounslow, 1998; Rigopoulos and Jones, 2003) for aggregation accommodate fragmentation as well. The latter involves an integral term, but its treatment is nevertheless simpler than that of aggregation (due to the lack of a convolution-like form). However, certain works have focussed on the fragmentation equation only, employing concepts in line with those in the above categories. Examples include Hill and Ng (1995) - which is based on the concept of the discrete equivalent equation and use of correction factors, and the works of Kumar et al. (2015) and Singh and Walker (2022) - which are based on the finite volume method and include an analysis of the convergence properties of the method. Several works have also compared discretisation methods for aggregation and fragmentation, these include Kostoglou and Karabelas (1994) and Vanni (2000).

The treatment of growth problems, whether alone or in conjunction with aggregation and/or fragmentation, presents a different numerical challenge: that of numerical diffusion. The growth term renders the PBE a first-order hyperbolic equation. Several solutions have been proposed for this problem, including methods based on the method of characteristics (Tsang and Brock, 1982; Kumar and Ramkrishna, 1997; Campos and Lage, 2003), hybrid stationary/moving grid methods (Jacobson, 1997), total variation diminishing (TVD) schemes (Ma et al., 2002; Qamar et al., 2006), an adaptive grid (in the particle size domain) for the spatially inhomogeneous PBE (Sewerin and Rigopoulos, 2017a) which was later coupled with the equations of fluid dynamics (Sewerin and Rigopoulos, 2017b; Sewerin and Rigopoulos, 2018), a hybrid Monte Carlo - discretisation method (Bouaniche et al., 2019) and a method based on an embedded reduced order representation (Sewerin, 2022).

It is clear that the solution of the PBE by discretisation poses several distinct challenges, and that different methods may prioritise different aspects - sometimes at the expense of other ones. The conservation of moments, accurate prediction of the distribution, mitigation of numerical diffusion, and the ability to deal with an arbitrary grid, can all compete and conflict with each other in the choice of a numerical method for solving the PBE. The present paper is the latest in a line of research seeking a method that addresses as many of these needs as possible. In particular, we aim to provide a method that allows for accurate solution of the PBE with all processes present, namely aggregation, fragmentation, nucleation and growth, while at the same time being conservative with respect to the total volume (or equivalently mass) of the particles in aggregation and fragmentation, as the particle volume should be invariant in these two processes. We also aim for the method to be applicable to an arbitrary grid, and sufficiently inexpensive computationally to allow for its incorporation in CFD-PBE implementations.

The essence of the approach presented here is to apply the finite volume method to the PBE, and compute the double integrals that arise from aggregation and fragmentation processes as fluxes of particles between different parts of the size domain, such that the birth and death terms are balanced. This was the concept behind the method of Liu and Rigopoulos (2019) for aggregation problems, which was applied to the modelling of soot formation and aggregation in flames (Liu and Rigopoulos, 2019; Liu et al., 2020; Sun et al., 2021). In the present work, the derivation of the method is presented in a more general way, as well as illustrated with a graphical procedure that illuminates the main concepts and facilitates its implementation. Another aim of this paper is to analyse the origin of the conservation error in finite element/volume methods, and show how it is overcome in the present method. In particular, it is shown that the double integrals are partitioned in such a way that the integration of the aggregation birth term is exact, and the only remaining approximation is the integration of the kernel. With respect to the latter, a Gaussian quadrature approach is employed and tested here in addition to our previous one-point integration. Subsequently, the method is extended to the discretisation of fragmentation processes. Finally, an improved scheme for the coupling of method with TVD schemes for growth discretisation is presented. Altogether, the method is able to deal with the solution of the PBE with any combination of kinetic processes and can also be coupled with fluid dynamics and CFD.

The paper is organised as follows. First, the discretisation of the aggregation terms is shown, together with a discussion of the nature of the problems involved in applying the finite volume method to the integral terms in the aggregation PBE. Subsequently, the discretisation of fragmentation and the combination with nucleation and growth are presented. The paper culminates with a number of test cases where the method is validated by comparing numerical solutions against known analytical and similarity solutions, as well as highly accurate solutions arising from the use of the discrete PBE.

2. The conservative finite volume method for aggregation

2.1. The aggregation PBE

First consider the discretisation of the aggregation terms. To this end, the population balance for a pure aggregation process, comprising a birth and a death term at the right-hand side is presented:

$$\frac{\partial n(v,t)}{\partial t} = \underbrace{\frac{1}{2}\int_0^v \beta(w, v-w)n(w)n(v-w)dw}_{\text{Birth term}} - \underbrace{n(v)\int_0^\infty \beta(v,w)n(w)dw}_{\text{Death term}} \tag{2}$$

The kernel, $\beta(v,w)$, encapsulates the physical mechanism of the aggregation process and may assume several forms corresponding to, for example, aggregation due to Brownian motion or shear; its particular form will not play any role in the derivation of the discretisation method. Aggregation poses a difficult problem for

discretisation methods, largely because of the non-linear birth integral term. This term is treated with numerical quadrature in the finite element or finite volume methods that belong to the second group of the classification presented in Section 1. Methods in this group face a difficulty with respect to the conservation of moments, the reasons for which will be discussed in Section 2.1. The essence of the method presented here is to ensure that the domain of this integral is partitioned in such a way that the product of number densities is constant within each partition. As such, the integration of this term is exact apart from the treatment of the kernel, which may still require numerical quadrature if it is nonlinear. This is a task that can be accomplished with high accuracy, as will be shown in Section 5.8. Therefore, the only remaining reason for discrepancies in the present method is the discrete representation of the distribution, which is the case with all discretisation methods, and can be controlled by refining the grid or using a higher order approximation of the distribution within each interval.

The shape of the resulting aggregates does not play any role in the development of the present method. The simplest case is coalescence to spherical particles, but fractal aggregates can also be considered via a suitable formulation of the kernel. If it is desirable to consider the shape and surface area of aggregates, then Eq. 2 must be either expanded into a two-dimensional population balance equation, or augmented by an additional equations for surface area or number of particles per aggregate. A numerical method for a two-PBE formulation based on the same principles as the method presented here can be found in Sun et al. (2021).

Before proceeding, Eq. 2 is recast into a more convenient form. First, the factor of $1/2$ in the birth term can be omitted by changing the limits of integration, and hence, not double counting particle combinations. This results in considerable savings in CPU time. Second, the semi-infinite domain is truncated to $[v_{min}, v_{max}]$, with v_{min} and v_{max} being the smallest and largest possible particle volumes. This truncation is necessary in order to develop a numerical solution method, although it implies that the equation is no longer strictly conservative, as particles may aggregate out of the domain. In practice, this loss of mass is negligible due to the very small number of such collision events - if this is not the case, this indicates that v_{max} was not chosen appropriately. In particular, v_{max} must represents a point at the tail of the distribution where the number density is expected to be practically zero - based on the physics of the process being considered. Finally, the equation is multiplied by particle volume, in preparation for the development of a method that conserves particle volume or volume fraction. It should be noted that if the equation is multiplied by v^k, the method will instead conserve the k-th moment of the distribution. With all these considerations, the resulting equation is:

$$\begin{aligned}\frac{\partial}{\partial t}(vn(v,t)) = &\int_{v_{min}}^{\frac{v}{2}} v\beta(w, v-w)n(w,t)n(v-w,t)dw \\ &- vn(v,t)\int_{v_{min}}^{v_{max}} \beta(v,w)n(w,t)dw\end{aligned} \tag{3}$$

Next, a grid of points, $v_i \in [v_{min}, v_{max}]$, is generated. The finite volume cells will be denoted as $\Delta v_i = v_i - v_{i-1}$, where $i \in (0, m)$. The method to be derived is applicable to an arbitrary grid.

2.2. A note on the finite volume method

The finite volume method has found most of its applications in the field of fluid mechanics, largely because it enforces conservation of mass. This is particularly important in fluid mechanics because mass flows from one part of the domain to another. Conservation of mass is also important for aggregation and fragmentation because mass is invariant in these processes. Furthermore, in a population balance formulation that includes aggregation, fragmentation and growth, ensuring conservation of mass in the first two processes provides the foundation for the correct prediction of mass change due to growth. These facts provide the motivation for adapting the finite volume method to the solution of the PBE. However, the application of the method to aggregation and fragmentation (particularly to the former) is by no means straightforward.

The basic concept of the finite volume method is to discretise the domain into a grid of cells, or size intervals in the case of the PBE, and to consider for each interval, the fluxes of mass into or out of the interval. By focussing on fluxes (rather than integrating over the intervals with weight functions, as in finite element methods), the method attains conservation of mass because every flux represents both an outflow from one interval, and an inflow into another. This is easy to attain in fluid mechanics, where the fluxes are constrained between neighbouring intervals.

Two complications arise when the finite volume method is applied to aggregation and fragmentation in a straightforward manner. First, the fluxes into an interval do not originate solely from its neighbours; rather, they may originate anywhere in the domain where particles are smaller, in the case of aggregation - or larger, in the case of fragmentation. The second issue is particular to aggregation, whose birth term resembles a convolution. This term does not permit separating the fluxes, and identifying their sources. These problems are more pronounced when dealing with arbitrary grids. The present method addresses the first of these issues by constructing a map of the aggregation and fragmentation fluxes, and the second one via a coordinate transformation that allows delineating of the fluxes, and finding their sources. These concepts are explained in the following sections.

2.3. Discretisation of the aggregation PBE via the finite volume method

The first step in the discretisation process with the finite volume method is to integrate Eq. 3 over an interval, Δv_i:

$$\begin{aligned}&\frac{d}{dt}\int_{v_{i-1}}^{v_i} vn(v,t)dv \\ &= \int_{v_{i-1}}^{v_i}\int_{v_{min}}^{\frac{v}{2}} v\beta(w, v-w)n(w,t)n(v-w,t)dwdv \\ &\quad - \int_{v_{i-1}}^{v_i} n(v,t)\int_{v_{min}}^{v_{max}} v\beta(v,w)n(w,t)dwdv\end{aligned} \tag{4}$$

The particle size distribution is now approximated as a piecewise constant function with constant value within each interval, i.e. $n(v) = n_i$ for $v_{i-1} < v \leqslant v_i$, as is customary in finite volume methods:

$$\begin{aligned}\hat{v}_i\frac{dn_i}{dt} = &\int_{v_{i-1}}^{v_i}\int_{v_{min}}^{\frac{v}{2}} v\beta(w, v-w)n(w,t)n(v-w,t)dwdv \\ &- n_i\int_{v_{i-1}}^{v_i}\int_{v_{min}}^{v_{max}} v\beta(v,w)n(w,t)dwdv\end{aligned} \tag{5}$$

where:

$$\hat{v}_i = \frac{v_i^2 - v_{i-1}^2}{2} \tag{6}$$

As mentioned in Section 2.2, the essence of a finite volume method is to compute a single flux for every mass exchange, thus ensuring that all inflows and outflows are balanced. These fluxes are most easily identified in the death term, which can be expressed in the following way:

$$\begin{aligned}&n_i\int_{v_{i-1}}^{v_i}\int_{v_{min}}^{v_{max}} v\beta(v,w)n(w,t)dwdv \\ &= \sum_{j=1}^{m}\left(n_i n_j\int_{v_{i-1}}^{v_i}\int_{w_{j-1}}^{w_j} v\beta(v,w)dwdv\right)\end{aligned} \tag{7}$$

where each term in the sum on the right-hand side is an individual death flux.

In order to illustrate the correspondence of birth and death fluxes, let us consider the aggregation of two parent particles in intervals Δw_j and Δw_k, forming a daughter particle in interval Δv_i. The following relationship can be written about the fluxes:

$$B_i = D_j + D_k \tag{8}$$

where B_i is the birth flux into interval Δv_i, while D_j and D_k are the death fluxes from intervals Δw_j and Δw_k, respectively. This relationship is represented schematically in Fig. 1. While the death fluxes can be easily identified and related to the intervals they originate in, the convolution-like form of the birth term in Eq. 5 prevents its splitting into its constituent fluxes. This term is thus responsible for the complexity in the discretisation of the aggregation PBE.

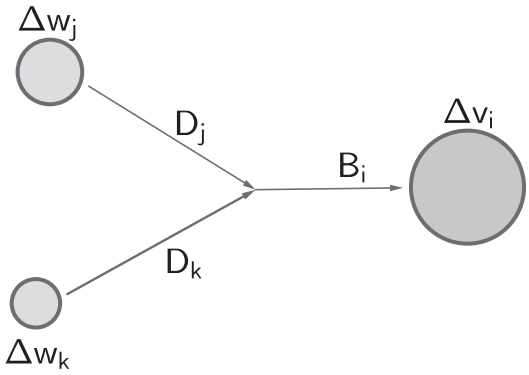

Fig. 1. Schematic of the aggregation-triplet of particles sizes: $\Delta w_k, \Delta w_j$ and Δv_i.

2.4. Transformation of the aggregation birth term

A transformation is now employed to delineate the contributions to the aggregation birth term, and map them to the death fluxes. Let v be the volume of the daughter particle and u, w be the volumes of the parent particles, such that $v = u + w$. By applying the change of coordinate $u = v - w$ to the birth term integral in Eq. 4, the integral is split into two terms that describe the birth of particles in interval Δv_i due to the constituent death terms in the corresponding parent intervals. This transformation was first introduced by Thompson (1968) in order to derive a closed equation for the moments of the aggregation PBE. Noting that the Jacobian of this transformation is 1, the resulting equation is:

$$\begin{aligned}\hat{v}_i \frac{dn_i}{dt} = &\int_{v_{i-1}-w}^{v_i-w} \int_{v_{min}}^{\frac{u+w}{2}} u\beta(w',u)n(w',t)n(u,t)dw'du \\ &+ \int_{v_{i-1}-w}^{v_i-w} \int_{v_{min}}^{\frac{u+w}{2}} w'\beta(w',u)n(w',t)n(u,t)dw'du \\ &- \sum_{j=1}^{m}\left(n_i n_j \int_{v_{i-1}}^{v_i} \int_{w_{j-1}}^{w_j} v\beta(v,w)dwdv\right)\end{aligned} \tag{9}$$

The convolution-like birth term has now been transformed into two terms of similar form to the death term, which correspond to its constituent death fluxes, as indicated by Eq. 8[1]. By considering the set of death fluxes and their corresponding aggregation triplets, it is now possible to construct the entire set of discretised equations, in the spirit of the finite volume method.

The final step is to convert the two birth integrals in Eq. 9 into sums of fluxes, as we did for the death integral in Eq. 7, and to map the regions where the death fluxes originate to the regions where they contribute. This mapping will be called the *aggregation map*.

2.5. Construction of the aggregation map

First note, that the two integrals corresponding to the birth term on the RHS of Eq. 9 are both over the same region in *w-u* space, which will be called the *parent space*. The region of integration represented by the limits of the double integrals in the birth term is shown in Fig. 2 as a shaded region. This region corresponds to the birth of particles in the interval Δv_i; a set of regions with similar shapes can be constructed for the birth terms in all other intervals.

It can be seen in Fig. 2 that, in an arbitrary grid, the boundaries of the shaded region do not coincide with the grid nodes. Therefore, an *auxiliary grid* of *complementary nodes* is introduced that allows this region to be partitioned into smaller ones, such that their boundaries coincide with the grid nodes. For a daughter interval, Δv_i, and a parent interval, Δw_j, the complementary nodes are defined as follows:

$$U_1 = v_{i-1} - w_j \tag{10a}$$

$$U_2 = v_{i-1} - w_{j-1} \tag{10b}$$

$$U_3 = v_i - w_j \tag{10c}$$

$$U_4 = v_i - w_{j-1} \tag{10d}$$

These nodes are shown in Fig. 3 and indicate complementary parent particle sizes that aggregate with the particles found at the outer boundaries of the parent interval that combines with Δw_j in order to form daughter particles at the boundaries of Δv_i. Every combination of Δv_i and Δw_j requires a new and unique set of complementary nodes, and thus the complementary nodes form a two-dimensional array, $U_k(\Delta v_i, \Delta w_j)$. Fig. 3 shows the region of integration in the parent space for a single combination of Δv_i and Δw_j, as well as the auxiliary grid corresponding to this particular combination (which is only part of the total integration region for the birth term in Δv_i, shown in Fig. 3). The fully partitioned aggregation map is shown in Fig. 4.

Owing to the approximation of the distribution via pairwise constant functions, the birth term can now be split into a sum of terms involving products of constant number densities. Each of these terms corresponds to an integration region with a certain shape and integration limits. For brevity, only a few shapes will be discussed here in detail, while the method for deriving the remaining shapes is analogous. The complete list of shapes that may appear on an arbitrary grid is shown in Appendix A.

Consider, the grid shown in Fig. 5. Three shapes can be identified, indicated as A, B_1 and B_2. The birth term integral over sub-region A takes the following form:

$$\begin{aligned}I_A = &n_j n_k \int_{w_{j-1}}^{w_j} \int_{v_{i-1}-w'}^{U_2} u\beta(w',u)dudw' \\ &+ n_j n_k \int_{w_{j-1}}^{w_j} \int_{v_{i-1}-w'}^{U_2} w'\beta(w',u)dudw'\end{aligned} \tag{11}$$

Considering now the rest of the shaded region, it can be seen that it is crossed by a grid node boundary. Therefore, the region is split into the two sub-regions B_1 and B_2, each corresponding to a different product of number densities:

$$I_{B_1} = n_j n_k \int_{w_{j-1}}^{w_j} \int_{U_2}^{u_k} u\beta(w',u)dudw' + n_j n_k \int_{w_{j-1}}^{w_j} \int_{U_2}^{u_k} w'\beta(w',u)dudw' \tag{12a}$$

[1] Note that the double integral must be further partitioned before being evaluated, which will result in the limits of the outer integral becoming constant - see also Eq. 11.

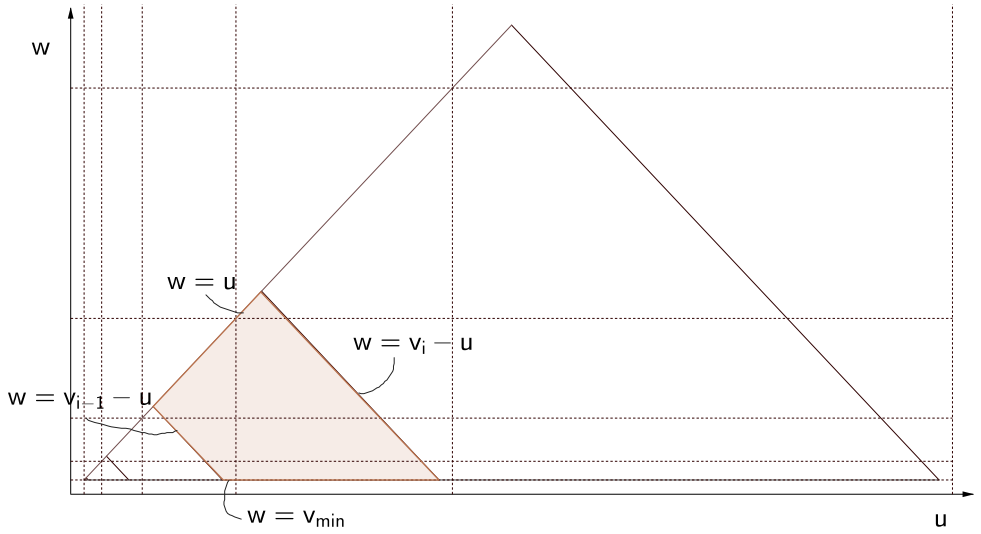

Fig. 2. Depiction of parent space, with the shaded region representing the region of integration for a given daughter interval, Δv_i. The dotted lines represent the grid in two dimensions.

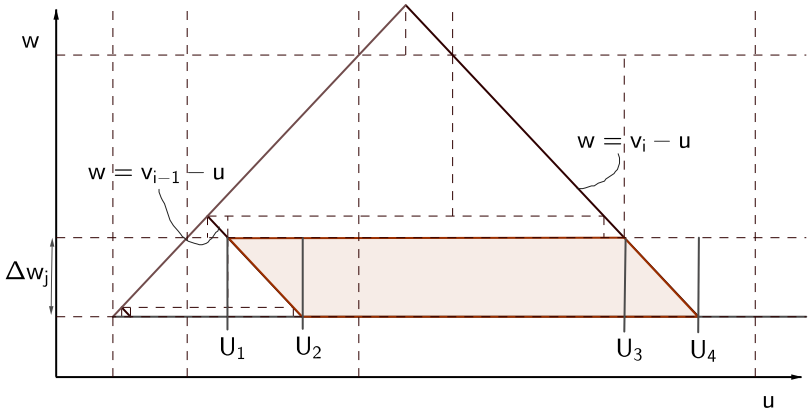

Fig. 3. A single combination of Δv_i and Δw_j leading to an auxiliary grid $U_k(\Delta v_i, \Delta w_j)$. The shaded region indicates the region of integration for the chosen combination of intervals, which is a part of the integration region for the birth term in Δv_i.

$$I_{B_2} = n_j n_{k+1} \int_{w_{j-1}}^{w_j} \int_{u_k}^{U_3} u\beta(w', u) du dw' + n_j n_{k+1} \int_{w_{j-1}}^{w_j} \int_{u_k}^{U_3} w'\beta(w', u) du dw' \tag{12b}$$

In order to generalise this procedure, let S represent the region of integration in the aggregation birth term for interval i. This region is partitioned into $P(i)$ sub-regions such that the number density products are constant over each sub-region, with each sub-region denoted by S_p where $p \in \{1, 2, 3 \ldots, P(i)\}$. The complete discretised equation takes the following form:

$$\hat{v}_i \frac{dn_i}{dt} = \sum_{p=1}^{P(i)} \left(n_{j(p)} n_{k(p)} \underbrace{\int_{S_p} u\beta(w', u) dw' du}_{I_{k(p)}} + n_{j(p)} n_{k(p)} \underbrace{\int_{S_p} w'\beta(w', u) dw' du}_{I_{j(p)}} \right) - \sum_{j=1}^{m} \left(n_i n_j \int_{v_{i-1}}^{v_i} \int_{w_{j-1}}^{w_j} v\beta(v, w) dw dv \right) \tag{13}$$

where P(i) is the total number of integration shapes that contribute to the birth term in daughter interval Δv_i. The products $n_{j(p)} n_{k(p)} I_{j(p)}$ and $n_{j(p)} n_{k(p)} I_{k(p)}$ represent the individual death terms from the two parents intervals of an aggregation triplet. The construction of the aggregation map, therefore, involves locating and classifying the sub-regions of integration such that the number density product is constant over each region.

The final step is the numerical evaluation of the integrals in Eq. 13. In previous work (Liu and Rigopoulos, 2019), these integrals were evaluated at a single point and weighted by the shape area. Here, to achieve higher accuracy, a two-dimensional, three-point Gaussian integration rule is employed. More details on the implementation of this rule are shown in Appendix B.

All operations involved in the construction of the aggregation map, i.e. the location and classification of sub-regions and the evaluation of integrals, are carried out once in the beginning of the computation, and the results are tabulated. Thus, the operations that must be carried out during each time step consist only of the time advancement of the discretised number densities. The procedure for the construction of the map can be summarised as follows:

1. Generate a grid, $v_i = [v_{min}, v_{max}]$, with $m + 1$ total points and m finite volume intervals, defined as $\Delta v_i = v_i - v_{i-1}$.
2. Locate shapes S_p using a nested loop - one loop for all daughter intervals and one for all parent intervals:
   - Establish the auxiliary grid for each combination of daughter and parent interval, $U_K(\Delta v_i, \Delta w_j)$.

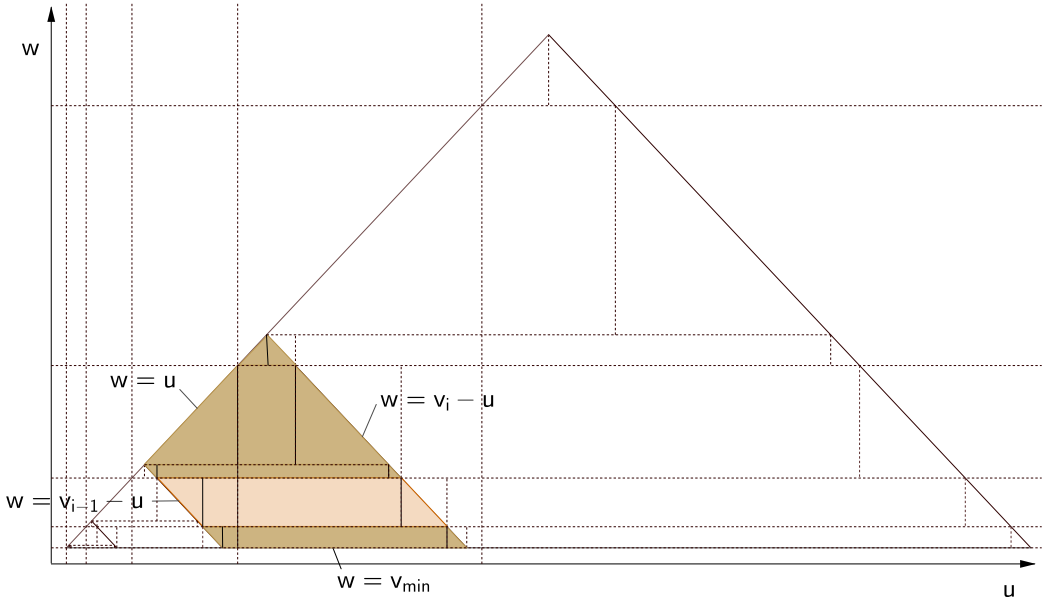

Fig. 4. The fully partitioned aggregation map. All possible daughter intervals are shown, and the total shaded region indicates the same region of integration as in Fig. 2. The lighter shaded region is the same region illustrated in Fig. 3.

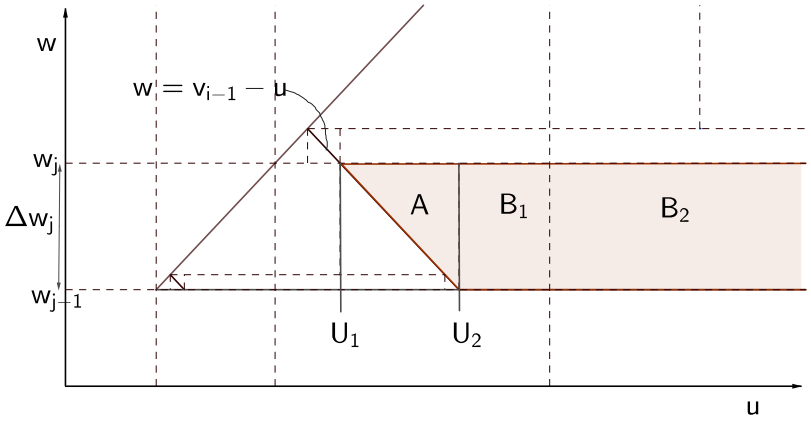

Fig. 5. Close view of an individual combination of parent intervals and associated sub-partitioning of the rectangular middle section. The vertical dotted line separating B_1 and B_2 corresponds to u_k, which is a further sub-partitioning node used in Eq. 12a,b.

- Locate and classify the sub-regions or shapes of constant number density pairs, S_p.
- Calculate the integrals $I_{j(p)}$ and $I_{k(p)}$.
- Store the aggregation integrals. For convenience, all unique combinations $\{i, j, k, I_j, I_k\}$ may be stored into a single array and indexed by a global pointer (as opposed to using local indices within each interval Δv_i).

2.6. Time advancement

The time advancement of Eq. 13 can be carried out with any temporal discretisation method. An explicit Euler method is used in the present work, as the equations are not stiff. For this implementation, the procedure to be carried out at each time step is summarised in the following algorithm, while the equations shown can be easily modified for other time advancement schemes.

1. For every interval, at time step n, the death terms $D^n_{j(p)}$ and $D^n_{k(p)}$ in all other parts of the domain to which particles contribute to the given interval are calculated as follows:

$$D^n_{j(p)} = n^n_{j(p)} n^n_{k(p)} I_{j(p)} \tag{14a}$$

$$D^n_{k(p)} = n^n_{j(p)} n^n_{k(p)} I_{k(p)} \tag{14b}$$

2. The birth terms at time step n are computed by summing the relevant death terms:

$$B^n_{i(p)} = D^n_{j(p)} + D^n_{k(p)} \tag{15}$$

where $B^n_{i(p)}$ is the birth term arising from the death terms $D_{j(p)}$ and $D_{k(p)}$.

3. The number densities at time step $n+1$ are now updated into temporary values (denoted by a star) as follows:

$$n^{n+1,*}_i = n^n_i + \frac{B^n_{i(p)}}{\hat{v}_{i(p)}} \delta t \tag{16a}$$

$$n^{n+1,*}_{j(p)} = n^n_{j(p)} - \frac{D^n_{j(p)}}{\hat{v}_{j(p)}} \delta t \tag{16b}$$

$$n^{n+1,*}_{k(p)} = n^n_{k(p)} - \frac{D^n_{k(p)}}{\hat{v}_{k(p)}} \delta t \tag{16c}$$

where $\hat{v}_{i(p)}$, $\hat{v}_{j(p)}$ and $\hat{v}_{k(p)}$ are defined as in Eq. 6.

This process is repeated for all aggregation triplets. At the end, the number density at time step $n+1$ has been calculated as follows:

$$n_i^{n+1} = n_i^n + \frac{1}{\hat{v}_i}\sum_{p=1}^{P(i)} B^n_{i(p)}\delta t - \frac{n_i^n}{\hat{v}_i}\sum_{j=1}^{m} n_j^n \int_{v_{i-1}}^{v_i}\int_{w_{j-1}}^{w_j} v\beta(v,w)dwdv\delta t \tag{17}$$

3. The conservative finite volume method for fragmentation

3.1. The fragmentation PBE

Fragmentation, or breakage, can be viewed as the mirror image of aggregation. Whereas in aggregation smaller parent particles combine to form a larger daughter particle, in fragmentation a single larger parent particle breaks apart to form two or more smaller daughter particles. When there are only two daughter particles, the process is often described as binary fragmentation. The PBE for a pure fragmentation process is shown below:

$$\frac{\partial n(v,t)}{\partial t} = \underbrace{\int_{v_{min}}^{\infty}\gamma(z)p(v,z)n(z,t)dz}_{\text{Birth term}} - \underbrace{\gamma(v)n(v,t)}_{\text{Death term}} \tag{18}$$

where $\gamma(v)$ is the fragmentation kernel, while $p(v,z)$ is the daughter particle size distribution. As was done in Section 2.1 with the aggregation PBE, Eq. 18 is first multiplied by particle volume in order to ensure conservation of volume, and furthermore the integral is truncated to v_{max}:

$$\frac{\partial}{\partial t}(vn(v,t)) = v\int_{v}^{v_{max}}\gamma(z)p(v,z)n(z,t)dw - v\gamma(v)n(v,t) \tag{19}$$

The following derivation has many analogies to the one presented in Section 2, and will thus be more concise. However, some key differences arise with fragmentation, and the discussion will focus on those.

3.2. Discretisation via the finite volume method

As in Section 2, a grid denoted as $v_i \in [v_{min}, v_{max}]$ is set up, with $\Delta v_i = v_i - v_{i-1}$. The lower truncation of the domain implies that fragmentation cannot proceed to infinitely smaller particles; this is ensured by the physics of the fragmentation process as embodied by the fragmentation kernel. Eq. 19 is now integrated across a finite volume interval:

$$\frac{d}{dt}\int_{v_{i-1}}^{v_i} vn(v,t)dv = \int_{v_{i-1}}^{v_i} v\int_{v}^{v_{max}}\gamma(z)p(v,z)n(z,t)dzdv - \int_{v_{i-1}}^{v_i} v\gamma(v)n(v,t)dv \tag{20}$$

or

$$\hat{v}_i\frac{dn_i}{dt} = \int_{v_{i-1}}^{v_i} v\int_{v}^{v_{max}}\gamma(z)p(v,z)n(z,t)dzdv - n_i\int_{v_{i-1}}^{v_i} v\gamma(v)dv \tag{21}$$

The same concept that was used in the discretisation of the aggregation terms to ensure conservation of particle volume is employed here. Only the fragmentation birth term is calculated, and the volume subtracted from the parent intervals is assigned to the appropriate daughter intervals. However, a key difference between fragmentation and aggregation arises when considering the double integral in Eq. 20. Whereas aggregation required a coordinate transformation to recast the aggregation birth term as a function of the two smaller parent sizes u and w, the fragmentation birth term can be readily used in its current form to construct the fragmentation map in z-v-space. This is because only one parent particle is involved in fragmentation, and thus the birth term does not have the convolution-like form encountered in aggregation. The construction of the fragmentation map is explained in the following section.

3.3. Construction of the fragmentation map

The fragmentation map is shown in Fig. 6. Only rectangular and triangular shapes arise, hence the fragmentation map is simpler than the aggregation one.

Consider any given triangular integration region along the line $z = v$. This class of shapes represents the contribution of parent particles from interval Δz_q fragmenting back into the very same interval. For the triangular regions along the line $z = v$, the parent and daughter interval are the same. When particles are removed

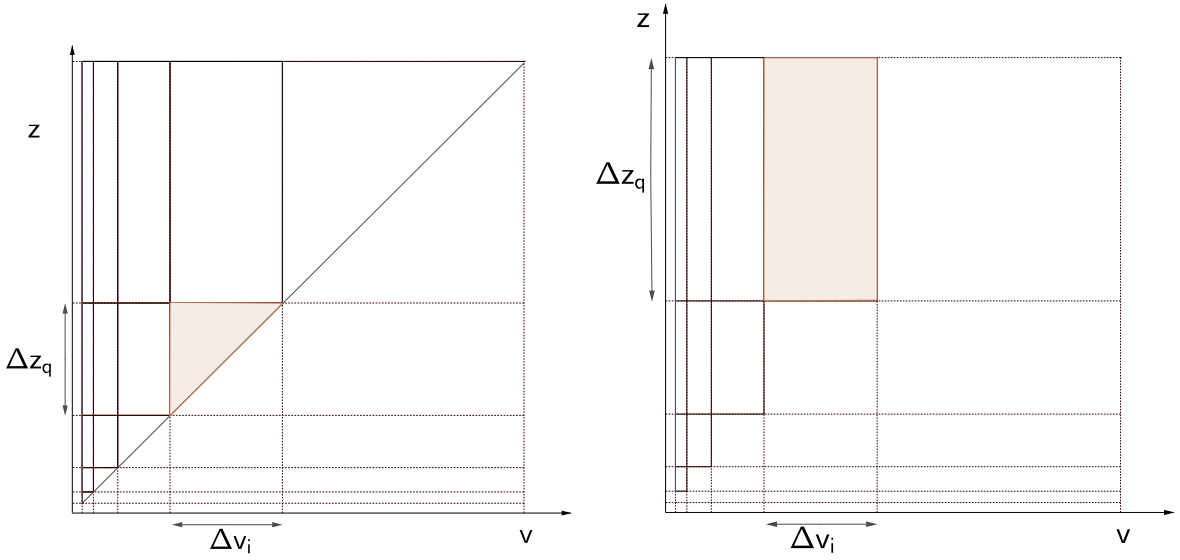

Fig. 6. a) Initial fragmentation map, showing all possible regions of integration in the parent-daughter space (or $z-v$-space). The shaded region indicates a triangular region along the line $z = v$, whose contribution can be ignored. b) Fragmentation map, showing all regions of integration. Only rectangular regions need to be considered.

and added back into the same interval, there is no net effect on the given interval number density, and thus it is not necessary to consider the contributions of the triangular sub-regions. The remaining rectangular regions represent the birth of mass into interval Δv_i as a result of the death of mass from several parent intervals Δz_q. For an individual parent-daughter interval pair, the required integral that needs to be evaluated numerically is shown in Eq. 22, where S_r represents the rectangular region with integration limits unique to index r, while q is the relevant parent interval that contributes mass to daughter interval Δv_i. The expression in Eq. 22 can be thought of as a constituent fragmentation birth term.

$$F_{q(r)} = n_{q(r)} \underbrace{\int_{S_r} v\gamma(z)p(v,z)dz\,dv}_{I_{q(r)}} \tag{22}$$

It is clear that further sub-partitioning of the integration shapes is not required when considering fragmentation, as every rectangular shape is already entirely within a region of constant number density. Furthermore, the fragmentation birth term is only a function of one number density per unique shape, as opposed to two in the context of aggregation. The fragmentation map, thus, consists of the set of triplets $\{i, q, I_z\}$, which are indexed by a pointer, as in aggregation. The fragmentation map is then tabulated and stored. The procedure for its construction can be summarised as follows:

1. Generate a grid, $v_i = [v_{min}, v_{max}]$, with $m+1$ total points and m finite volume intervals, with $\Delta v_i = v_i - v_{i-1}$
2. Locate the triangular shapes and remove them from the set of possible fragmentation integration regions (i.e. those where $i = q$).
3. Locate the rectangular integration regions using a nested loop - one loop over all daughter intervals and one over all possible parent intervals:
   - Calculate the integrals $I_{q(r)}$.
   - Create a unique pointer for each rectangular sub-region and store the fragmentation triplet, $\{i, q, I_{q(r)}\}$.

3.4. Time advancement

As with the case of aggregation, the time advancement procedure and relationships for fragmentation based on an explicit Euler method are shown below. The equations can be easily modified for another time-integration scheme.

1. For each interval i and time step n, the fragmentation birth terms, $F^n_{q(r)}$, are calculated using the tabulated integrals $I_{q(r)}$:

$$F^n_{q(r)} = n^n_{q(r)} I_{q(r)} \tag{23a}$$

2. The number densities at time step $n+1$ are now augmented as follows:

$$n_i^{n+1,*} = n_i^n + \frac{F^n_{q(r)}}{\hat{v}_i}\delta t \tag{24a}$$

$$n_q^{n+1,*} = n_q^n - \frac{F^n_{q(r)}}{\hat{v}_q}\delta t \tag{24b}$$

$$n_i^{n+1} = n_i^n + \frac{1}{\hat{v}_i}\left[\sum_{r=1}^{R(i)} F^n_{q(r)}\right]\delta t - \frac{1}{\hat{v}_i}\left[\sum_{s=1}^{S(i)} F^n_{q(s)}\right]\delta t \tag{25}$$

where $\hat{v}_i$ are defined as in Eq. 6. R(i) represents the number of integration shapes that contribute mass to interval Δv_i, and S(i) represents the number of shapes where Δv_i is the parent interval. Thus, in a similar manner to Eq. 16, the constituent fragmentation birth terms to other intervals where Δv_i is the parent, are reassembled to form the original death term in Eqn. 21.

4. Nucleation and growth

The treatment of the nucleation term does not pose any particular issue, apart from the need for a grid with sufficient resolution around the nuclei size. However, the presence of growth gives rise to the problem of numerical diffusion due to the hyperbolic nature of the resulting equation. A number of solutions have been proposed for this problem, from total variation diminishing (TVD) schemes (Ma et al., 2002; Qamar et al., 2006) to adaptive grid methods (Sewerin and Rigopoulos, 2017a). The discretisation method presented in the present work for aggregation and fragmentation can be combined with most of the existing schemes for growth. The coupling with a TVD scheme, such as the one of Qamar et al. (2006), is shown.

The PBE for a problem involving nucleation and growth as well as other processes can be written as follows:

$$\frac{\partial n(v,t)}{\partial t} + \frac{\partial [G(v)n(v,t)]}{\partial v} = B\delta(v - v_{nuc}) + S \tag{26}$$

where S is a source term accounting for aggregation and fragmentation. For a finite volume discretisation in terms of volume fraction, Eq. 26, is multiplied by v and integrated over an arbitrary interval Δv_i:

$$\begin{aligned}\frac{d}{dt}\int_{v_{i-1}}^{v_i} vn\,dv + \int_{v_{i-1}}^{v_i} v\frac{\partial [G(v)n(v)]}{\partial v}dv \\ = \int_{v_{i-1}}^{v_i} vB\delta(v - v_{nuc})dv + \int_{v_{i-1}}^{v_i} vS\,dv\end{aligned} \tag{27}$$

The treatment of nucleation is straightforward. If the nuclei volume is located within the first interval, we have:

$$\int_{v_{min}}^{v_1} vB\delta(v - v_{nuc})dv = v_{nuc}B \tag{28}$$

Rewriting the growth term using product rule and performing the integration yields the fluxes at the boundaries of interval Δv_i, as well as a new source term representing the addition of mass to the particles within Δv_i:

$$\int_{v_{i-1}}^{v_i} v\frac{\partial (G(v)n(v,t))}{\partial v}dv = [Gnv]_{v_i} - [Gnv]_{v_{i-1}} - \int_{v_{i-1}}^{v_i} Gn\,dv \tag{29}$$

In order to minimise numerical diffusion, the flux terms in Eq. 29 can be dealt with a TVD scheme, which approximates them as functions of values at neighbouring intervals and a flux limiter function. In the present work we employ the approach of Qamar et al. (2006, 2009), which is based on a TVD scheme due to Koren et al. (1993). The reader may refer to the above references for the derivation, and the final expression for the limiter is:

$$[G(v)nv]_{v_i} = v_i G(v_i)\left[n_{u(v_i)} + \frac{\phi(r_i)}{2}\left[n_{u(v_i)} - n_{uu(v_i)}\right]\right] \tag{30}$$

where $n_{u(v_i)}$ and $n_{uu(v_i)}$ are the number densities of the two intervals upstream of node v_i, and $\phi(r_i)$ is the flux limiter at node v_i given by:

$$\phi(r_i) = \max\left[0, \min\left[2r_i, \min\left[\frac{\frac{1}{3}v_i - v_{i-1}}{v_{m,i} - v_{m,i-1}} + \frac{2r_i}{3}\frac{v_i - v_{i-1}}{v_{m,i+1} - v_{m,i}}, 2\right]\right]\right] \tag{31}$$

where $v_{m,i} = 0.5(v_i + v_{i-1})$ and r_i is the upwind ratio of two consecutive number density gradients (Koren et al., 1993):

$$r_i = \frac{n_{i+1} - n_i + \epsilon}{n_i - n_{i-1} + \epsilon} \tag{32}$$

where ϵ is a small number employed to avoid division by zero.

The growth source term requires additional treatment. By multiplying and dividing by v, we obtain:

$$\int_{v_{i-1}}^{v_i} Gnd v = \int_{v_{i-1}}^{v_i} \frac{G}{v} n v dv \tag{33}$$

We now treat the integrand as a product of two functions, namely G/v and nv, and invoke the Mean Value Theorem for Integrals (see Spivak (1994), p. 274) to write the growth source term as follows:

$$\int_{v_{i-1}}^{v_i} \frac{G}{v} n v dv = \frac{G(\zeta)}{\zeta} \int_{v_{i-1}}^{v_i} n v dv = \frac{G(\zeta)}{\zeta} \hat{v}_i n_i \tag{34}$$

where $\zeta \in [v_{i-1}, v_i]$. While the theorem guarantees that a value of ζ exists, it does not help us to find it. We therefore approximate ζ with the midpoint of the interval and obtain:

$$\frac{G(\zeta)}{\zeta} \hat{v}_i n_i = \frac{G(v_{m,i})}{v_{m,i}} \hat{v}_i n_i \tag{35}$$

This reformulation of the TVD growth discretisation is necessary in order to ensure that the numerical scheme for growth has consistent number density definitions with that for aggregation-fragmentation. The latter is derived from a mass-based description, as the first moment is an invariant in these processes. However, in the case of pure growth, it is the total number density or zeroth moment that is invariant, while the mass increases over time. The original work of Qamar et al. (2006) uses a number-based definition for the discretised number densities. However, if that scheme is combined with a mass-based description, it can be shown that an error is introduced. By modifying the growth discretisation to be mass-based, this error can be avoided. A comparison of the two formulations on an aggregation-growth test case will be shown in Section 5.6.

5. Results and discussion

In order to validate the approach developed in the present paper, a series of test cases that have analytical solutions will now be considered. To extend the range of test cases, the numerical solution of the discrete PBE (DPBE) will also be employed for validation purposes, since it can be obtained with very high accuracy (albeit at high computational cost) and can thus be considered as equivalent to an analytical solution. The test cases are summarised in Table 1. Finally, an analysis of the accuracy of certain aspects of the method and of the computational performance will be carried out.

5.1. Aggregation

5.1.1. Analytical solutions

Very few analytical solutions have been obtained for aggregation problems. An analytical solution for the case of the constant kernel was first derived by Schumann (1940), while Scott (1968) carried out a comprehensive analytical study with several kernels. Here, we will employ the solutions in the form presented by Gelbard and Seinfeld (1978). The solutions are for the following exponential initial distribution:

$$n(v,0) = \frac{N_0}{v_0} e^{-v/v_0} \tag{36}$$

where N_0 is the initial number of particles and v_0 is the initial average particle volume. The first solution is for the constant kernel:

$$\beta(v,w) = \beta_0 \tag{37}$$

The solution is:

$$n(v) = \beta_0 \frac{4N_0}{(T+2)^2} \exp\left(-\frac{v}{v_0}\frac{2}{T+2}\right) \tag{38}$$

where T is a dimensionless time defined as follows:

$$T = \beta_0 N_0 t \tag{39}$$

The second solution is for the sum kernel:

$$\beta(v,w) = \beta_0 (v+w) \tag{40}$$

and the initial condition defined by Eq. 36. The solution is:

$$n(v) = \frac{N_0(1-T)}{vT^{1/2}} \exp\left[-(1+T)w\right] I_1\left(2wT^{1/2}\right) \tag{41}$$

where I_1 is the modified Bessel function of the first kind of order one, while the dimensionless time, T is defined as follows in this case:

$$T = \beta_0 N_0 v_0 t \tag{42}$$

Fig. 7 and Fig. 8 show excellent agreement with the analytical solutions describing the evolution of the particle size distribution. In these and the following figures, the notation due to Friedlander (2000) indicating the particle size dimension with l and the physical space dimensions with L is adopted.

5.2. Numerical solutions of the discrete PBE for problems with self-similarity

Since the number of population balance problems that have analytical solution is very limited, we will also compare with some solutions obtained with the discrete population balance equation (DPBE) for aggregation (Smoluchowski equation):

$$\frac{dn_1}{dt} = -n_1 \sum_{j=1}^{\infty} \beta_{ij} n_j \tag{43a}$$

$$\frac{dn_i}{dt} = \frac{1}{2} \sum_{j=1}^{i-1} \beta_{j,i-j} n_j n_{i-j} - n_i \sum_{j=1}^{\infty} \beta_{ij} n_j \qquad \forall i > 1 \tag{43b}$$

Solutions of this equation are equivalent to those of the continuous PBE for aggregation. Eqs. 43 can be solved with an explicit Euler method as follows:

Table 1
Summary of test cases.

Test Case	$\beta(v,w)$	$p(v,w)$	$\gamma(w)$	Growth	Reference solution
Aggregation, constant kernel	1	-	-	-	Gelbard and Seinfeld (1978)
Aggregation, sum kernel	$v+w$	-	-	-	Gelbard and Seinfeld (1978)
Aggregation, free-molecule kernel	$\left(\frac{1}{v}+\frac{1}{w}\right)^{0.5}\left(v^{\frac{1}{3}}+w^{\frac{1}{3}}\right)^2$	-	-	-	DPBE solver
Aggregation, Brownian kernel	$\left[\left(\frac{1}{v}\right)^{\frac{1}{3}}+\left(\frac{1}{w}\right)^{\frac{1}{3}}\right]^2$	-	-	-	DPBE solver
Ternary fragmentation	-	$\frac{6}{w}\left(1-\frac{v}{w}\right)$	w^2	-	Ziff (1991)
Uniform binary fragmentation	-	$\frac{2}{w}$	w	-	Ziff and McGrady (1985)
Aggregation-growth	1	-	-	$k_g v$	Ramabhadran et al. (1976)
Aggregation-fragmentation	1	$\frac{2}{w}$	$2w$	-	Lage (2002)

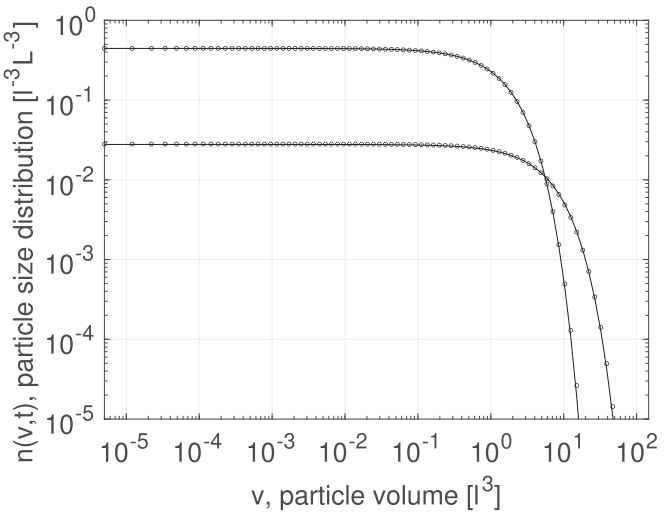

Fig. 7. Pure aggregation process using the constant aggregation kernel. Solid lines are the analytical solution, while square and triangular marks are the numerical solutions at 1 s and 10 s, respectively. 80 grid points were used, while β_0 = 1.

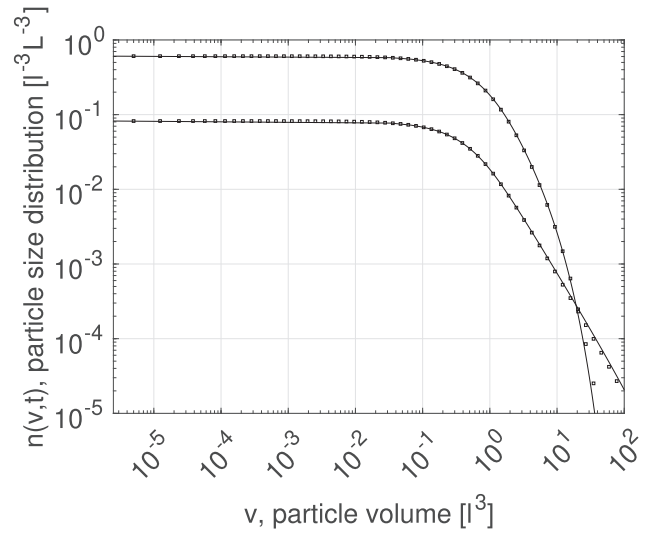

Fig. 8. Pure aggregation process using the sum aggregation kernel. Dashed lines are the analytical solution, while the square and triangular marks are the numerical solutions at 0.5 s and 2.5 s, respectively. 80 grid points were used, while β_0 =1.

$$n_i^{t+dt} = n_i^t + dt\left(\frac{1}{2}\sum_{j=1}^{i-1}\beta_{ij}n_j^t n_{i-j}^t - \beta_{ij}n_i^t\sum_{j=1}^{\infty}n_j^t\right) \tag{44}$$

While computationally expensive, the solution of the discrete equation with this direct method is very accurate and can be regarded as a substitute for an analytical solution, thus allowing us to employ any kernel and initial condition. We are particularly interested in two important kernels that appear in physical processes. The first one is the kernel for aggregation in the free molecular regime (Friedlander, 2000):

$$\beta(v,w) = \left(\frac{3}{4\pi}\right)^{1/6}\left(\frac{6kT}{\rho_p}\right)^{1/2}\left(\frac{1}{v}+\frac{1}{w}\right)^{1/2}\left(v^{1/3}+w^{1/3}\right)^2 \tag{45}$$

The second one is the kernel for aggregation due to Brownian motion (Friedlander, 2000):

$$\beta(v,w) = \frac{2kT}{3\mu}\left(\frac{1}{v^{1/3}}+\frac{1}{w^{1/3}}\right)\left(v^{1/3}+w^{1/3}\right) \tag{46}$$

In the above equations, k is the Boltzmann constant, ρ_p is the density of the particles and μ is the viscosity of the fluid. However, in the tests the entire multiplicative factor has been set equal to 1, as indicated in Table 1.

After sufficiently long time, an aggregation process with these kernels reaches a self-similar solution that is independent of the initial condition. Approximations to this solution have been derived analytically by Swift and Friedlander (1964, 1966, 1972) and numerically by Landgrebe and Pratsinis (1989). In the present work, this solution was obtained by a numerical solution of Eq. 43 using the discretisation method described by Eq. 44, as well as by solution of the continuous equation using our conservative finite volume method. The results are presented in terms of the following similarity variable:

$$\eta(t) = \frac{v}{v_m(t)} \tag{47}$$

where $v_m(t)$ is defined in terms of the zeroth and first moment as follows:

$$v_m(t) = \frac{M_1}{M_0(t)} \tag{48}$$

Note that M_1 is constant when only aggregation is present.

Fig. 9 shows a comparison of the two solutions for aggregation in the free molecule regime.80 grid nodes were employed for the solution of the continuous PBE with the conservative finite volume method, and excellent agreement obtained. Fig. 10 shows a comparison of the solutions for the Brownian kernel. Again, excellent agreement is observed. For both cases, the numerical solution of the discrete PBE involved the solution of 10,000 ODEs representing every possible particle size. As before, the first moment was conserved exactly in these two simulations.

5.3. Fragmentation

Ziff and McGrady (1985) considered binary fragmentation with a number of different initial conditions. An exponential initial particle size distribution was used for this work and the resulting solution and initial condition is shown in Eq. 49.

$$n(v,0) = \frac{N_0}{v_0}\exp\left[\frac{-v}{v_0}\right] \tag{49a}$$

$$n(v,t) = \left(1+t^2\right)\exp\left[-v(1+t)\right] \tag{49b}$$

where $N_0 = 1$ and $v_0 = 1$.

Ziff (1991) went further, and considered a general class of scaling solutions to the fragmentation equation that allowed for the treatment of a variety of fragmentation kernels as well as kernels that describe multiple fragments being produced. The special case of ternary fragmentation with a monodisperse initial condition is shown in Eq. 50:

$$n(v,0) = \delta(v - v_{max}) \tag{50a}$$

$$n(v,t) = \frac{1}{v_{max}}\exp\left[-tv_{max}^2\right]\delta(v - v_{max}) + 6tv\int_v^{v_{max}} y^{-2}\exp\left[-ty^3\right]dy \tag{50b}$$

Fig. 11, shows good agreement in the binary fragmentation case with 80 grid points. The particle size distribution is shown at t = 1 s and t = 10 s.

Fig. 12, shows good agreement with the analytical solution for batch ternary breakage.Fig. 13 and 14.

For both of these fragmentation test cases, it is important to highlight that there was no adjustment required to the numerical scheme, in terms of the fragmentation map or the integration calculations. Fragmentation kernels with multiple fragments - three

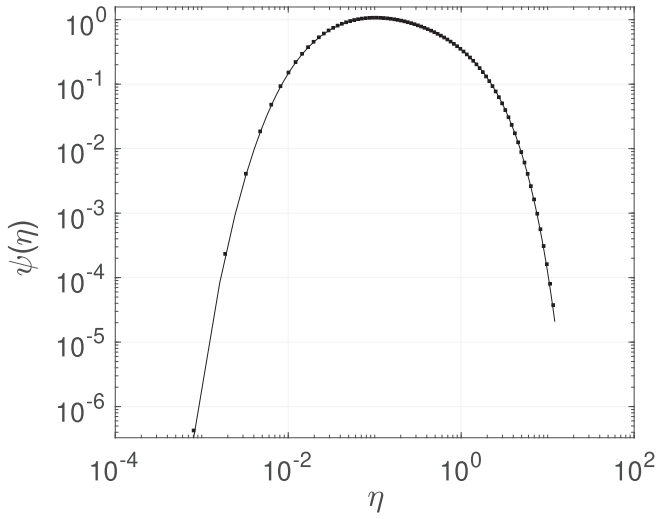

Fig. 9. Pure Aggregation with the free-molecule regime kernel, self-similar solution. The solid line is the DPBE solution and the points are the results with the present method. 80 grid points were used.

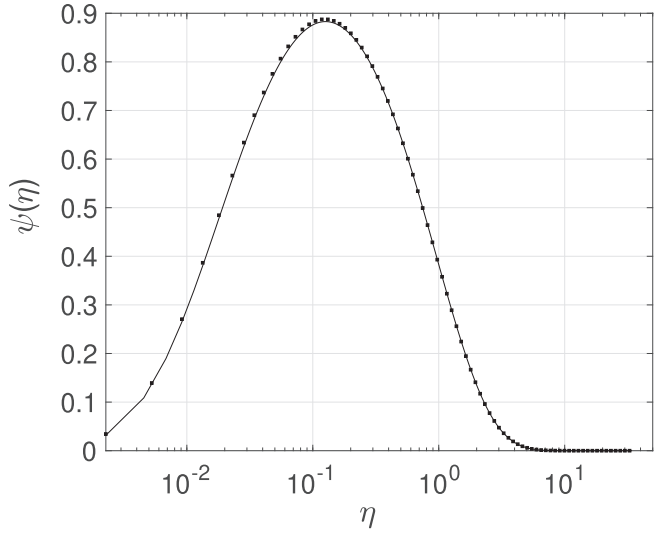

Fig. 10. Pure aggregation process using the Brownian aggregation kernel, self-similar solution. The solid line is the DPBE solution and the points are the results with the present method. 80 grid points were used.

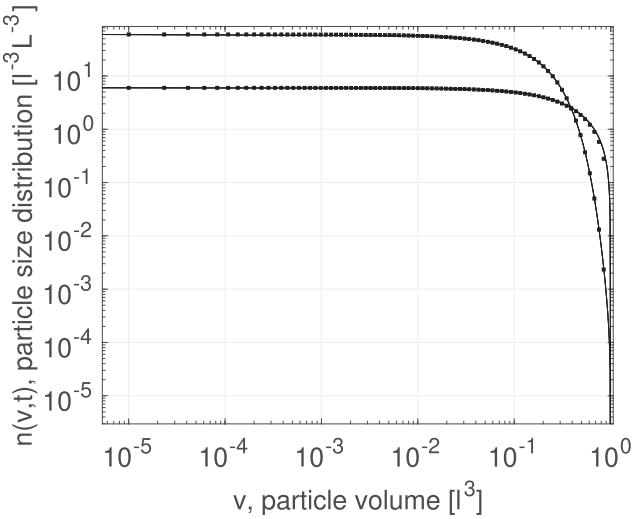

Fig. 11. Evolution of the particle size distribution for batch binary breakage; analytical and numerical solutions are shown for t = 1 s and t = 10 s. 80 grid points were used.

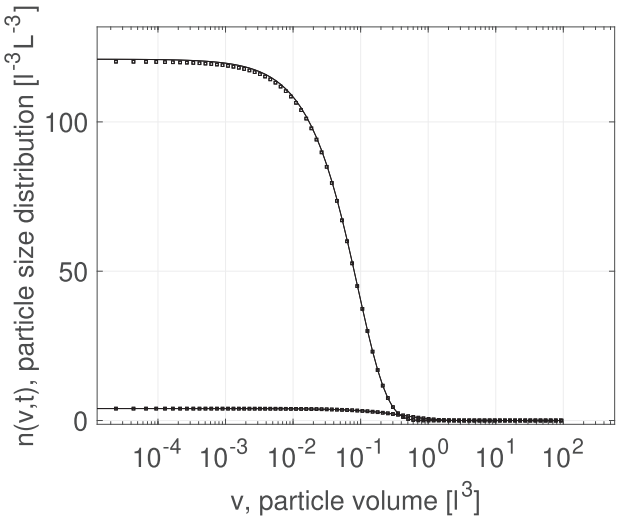

Fig. 12. Evolution of particle size distribution for batch ternary fragmentation; analytical and numerical solutions are shown for t = 1 s and t = 10 s. 80 grid points were used.

or more - can be solved for without need for any change in the implementation of the methodology.

5.4. Aggregation and fragmentation

In order to demonstrate the aggregation map and fragmentation map working together, we investigated a joint constant aggregation and uniform binary fragmentation problem that happens to be one of the few aggregation-fragmentation cases that have an analytical solution. The solution was derived by Patil and Andrews (1998) and corrected by Lage (2002). It describes the temporal evolution of the particle size distribution in non-dimensional terms for limited initial conditions. The joint constant aggregation and uniform binary breakage case will form a steady-state solution independent of the initial distribution, and it is this solution that will be the focus of this test case. Essentially, one of the initial conditions outlined in Lage (2002) is the steady-state solution itself - in which case the particle size distribution remains invariant for all time. A more challenging scenario is to initiate the distribution as either breakage-dominated or aggregation-dominated, and to compare with the steady-state behaviour of the distribution as well as its moments. The latter have analytical solutions for their steady-state behaviour, independent of the initial condition used. As the particle size distribution evolves to a steady-state solution, the zeroth moment becomes invariant. For every aggregation event where two particles become one larger particle, there is an equal and opposite fragmentation event where a large particle breaks into 2 smaller ones. The analytical solutions are shown in Appendix C.

The numerical scheme employing both aggregation and fragmentation maps accurately reproduces the steady-state solution, as well as crucially conserving mass and, once steady-state has been achieved, conserving total number density as well.

5.5. Aggregation and growth

Ramabhadran et al. (1976) considered a joint aggregation and growth case where the constant aggregation kernel and a linear

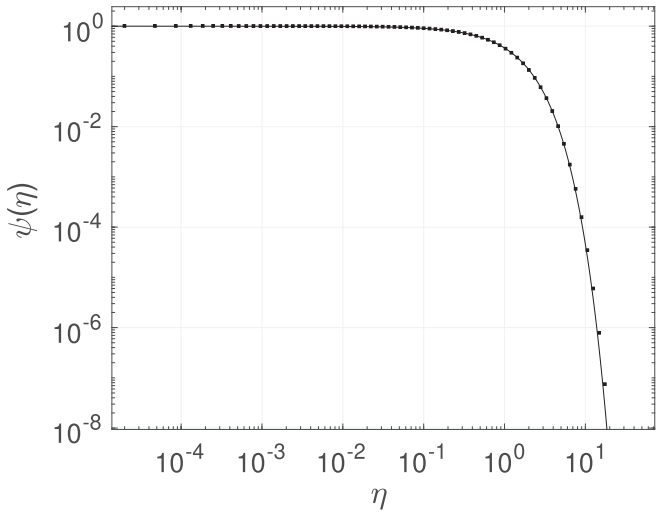

Fig. 13. Steady state solution of the joint aggregation-fragmentation test case (Lage, 2002); 80 grid points were used.

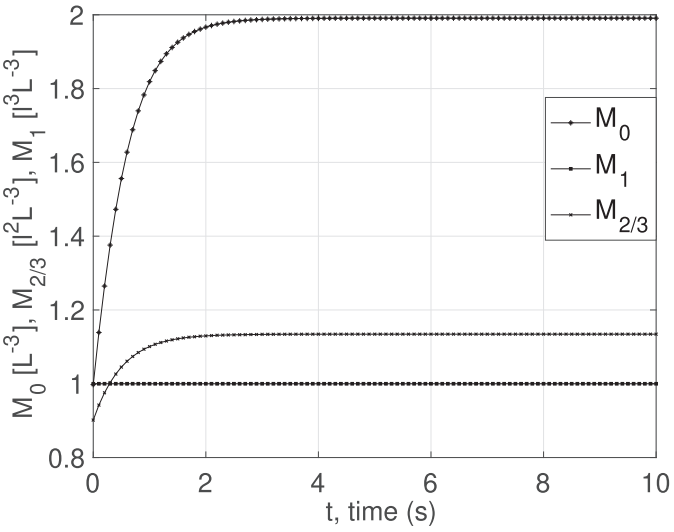

Fig. 14. Evolution of zeroth and first moments in joint aggregation-fragmentation test case. Note the total number density as well as the 2/3 moment becoming constant as the system evolves to a steady state.

size-dependent growth kernel ($G(v) = k_g v$) were used. The initial condition is again the exponential distribution Eq. 36. The solution for the number density involves the zeroth and first moments, for which equations have also been derived, as shown below:

$$n(v,t) = \frac{M_0^2}{M_1} \exp\left(-\frac{M_0}{M_1} v\right) \tag{51a}$$

$$M_0(t) = \frac{2N_0}{2 + \beta_0 N_0 t} \tag{51b}$$

$$M_1(t) = N_0 v_0 \exp(\sigma_1 t) \tag{51c}$$

The analytical solution is compared with the numerical solution with the conservative finite volume method obtained with 80 grid points in Fig. 15. The comparison between the two solutions is very good for all time instances considered, indicating that the aggregation discretisation method performs very well in the presence of growth.

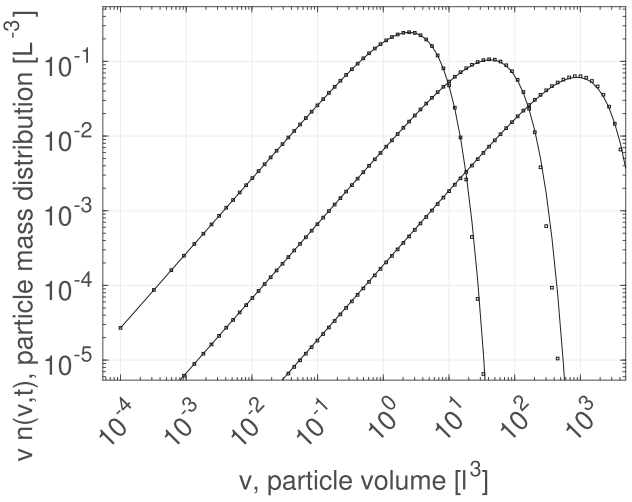

Fig. 15. Joint aggregation-growth test case. Constant aggregation kernel with a linear size-dependent growth kernel i.e. $G(v) = k_g v$ where in this case k_g = 0.5.

5.6. Mass-based versus number-based growth TVD scheme

As discussed in Section 4, in order to render the discretisation of the growth term fully consistent with that of aggregation and fragmentation, a mass-based formulation must be employed - which results in an extra source term. In order to examine this aspect of the method, the aggregation-growth test case was run twice, once using the original number-based TVD scheme for growth and once using the mass-based formulation. The zeroth, two-third (which is proportional to the particle surface area) and first moments were calculated and the results for various grids are shown in Fig. 16. It can be seen that the number-based scheme produces slightly more accurate predictions of the zeroth moment, with the error dropping below 1% with 60 intervals, while the same occurs with 80 intervals in the case of the mass-based formulation. However, the mass-based formulation considerably outperforms the number-based formulation when predicting the two-third moment, producing an error of roughly 1% with 60 intervals, as opposed to more than 100 intervals in the case of the latter. This is significant, as the two-third moment is important in problems involving surface chemistry such as crystallisation and flame synthesis of nanoparticles. Finally, with respect to the first moment, the mass-based formulation produces effectively zero error with all grids, confirming the conservation property of the method, while the CFV-TVD number-based formulation requires close to 200 intervals to achieve an error of less than 1%.

5.7. Accuracy of moment prediction

We will now examine the evolution of the moments as predicted by the conservative finite volume method. The moments to be examined are the zeroth moment (total number of particles), the two-third moment (proportional to the total particle surface area) and the first moment (total particle volume). The moment evolution will be considered for all test cases, and comparison will be made with analytical solutions or DPBE. In the aggregation-fragmentation test case, the steady-state moments will be compared with their analytical solution. In order to evaluate the mean error during the entire temporal evolution, the moments were evaluated at 100 instances for each test case.

The results are shown in Table 2. The errors are generally small and less than 1% in most cases. The largest errors appeared in the sum kernel and the aggregation-growth case which, exhibited an error of 0.78% and 0.83%, respectively. This can be expected given

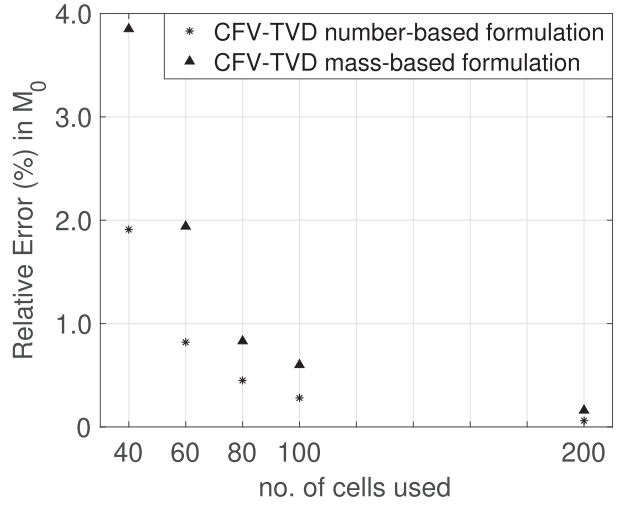

(a) Relative error (%) in zeroth moment M_0, in the aggregation-growth case

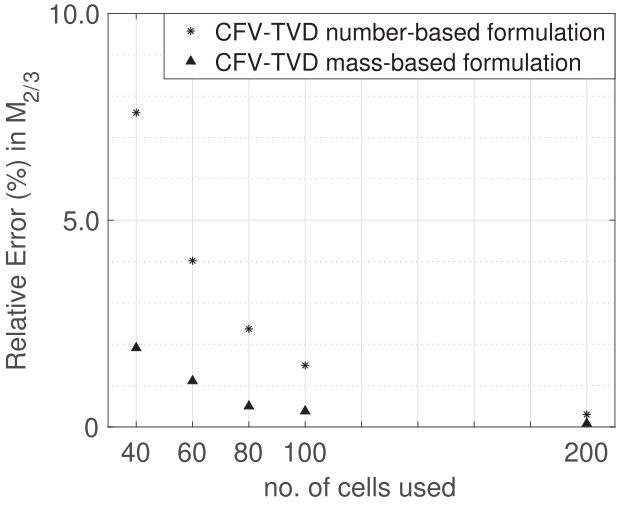

(b) Relative error (%) in two-thirds moment $M_{2/3}$, in the aggregation-growth case

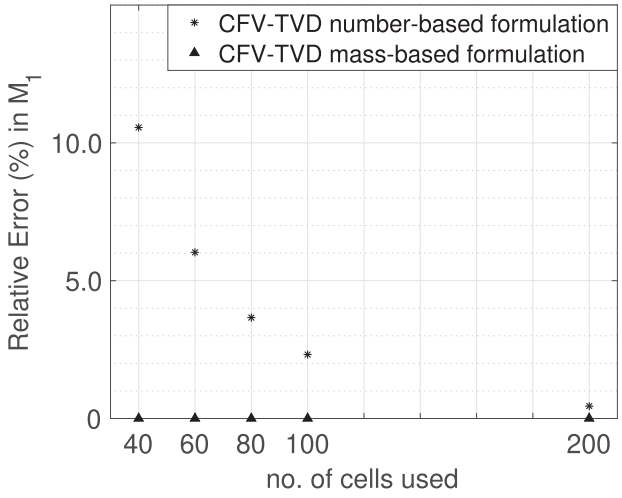

(c) Relative error (%) in first moment M_1, in the aggregation-growth case

Fig. 16. Relative error in the moments for the two differing joint aggregation-growth schemes as compared with the analytical moments equations. Note, the wholly mass-based formulation has zero relative error in M_1 for all grids used.

Table 2
Relative error in the moments of the particle size distribution, average over 100 time instances.

Test case	M_0	$M_{2/3}$	M_1	Intervals	$[v_{min}, v_{max}]$
Constant aggregation	0.30%	0.28%	0%	80	$\left[2.5 \cdot 10^{-6}, 1.6 \cdot 10^{2}\right]$
Sum aggregation	0.78%	1.11%	0%	80	$\left[5 \cdot 10^{-6}, 5 \cdot 10^{4}\right]$
Free-molecule aggregation	0.20%	0.18%	0%	80	$\left[10^{-1}, 1.5 \cdot 10^{4}\right]$
Brownian aggregation	0.12%	0.13%	0%	80	$\left[10^{-1}, 1.5 \cdot 10^{4}\right]$
Ternary fragmentation	0.30%	0.17%	0%	80	$\left[10^{-5}, 1\right]$
Uniform binary fragmentation	0.63%	0.29%	0%	80	$\left[10^{-5}, 10^{2}\right]$
Aggregation-growth	0.83%	0.50%	0%	80	$\left[0, 10^{4}\right]$
Aggregation-fragmentation	0.46%	0.27%	0%	80	$\left[10^{-5}, 5 \cdot 10^{1}\right]$

the fact that, the distribution moves rapitdly towards the right end of the domain where the grid is more coarse. The error in M_1 is always 0%, confirming the fact that the method is conservative by construction.

5.8. Accuracy of aggregation kernel integration

As mentioned in Section 2.1, the partitioning of the aggregation integral terms allows for exact evaluation of the number density

products, and the only approximation involved is the numerical integration of the kernel. Therefore, it is important to examine the accuracy involved in this step. In the present section, the relative error in the integration of four non-linear kernels, namely the free-molecule, Brownian, shear and gravitational kernel is investigated. The equations for the first two have already been shown (Eqs. 45 and 46, respectively). The kernel for laminar shear is:

$$\beta(v,w) = \frac{1}{\pi}\frac{du}{dx}\left(v^{1/3} + w^{1/3}\right)^3 \tag{52}$$

Finally, the gravitational kernel for small particles, creeping flow and continuum regime, is:

$$\beta(v,w) = \frac{\left(\rho_p - \rho\right)g}{6\mu}\left(\frac{3}{4\pi}\right)^{\frac{1}{3}}\left(v^{\frac{1}{3}} + w^{\frac{1}{3}}\right)^2\left|v^{\frac{2}{3}} - w^{\frac{2}{3}}\right| \tag{53}$$

More information on the physics of these kernels can be found in, Friedlander (2000). As before, only the volume-dependent part of the kernel will be considered, as the rest is a multiplicative factor that can be taken out of the integral.

For clarity, the integral in Eq. 11 is rewritten here in the following way:

$$I = n_{j(p)}n_{k(p)}\int\int_{S_p}(u + w\prime)\beta(w\prime, u)dudw\prime \tag{54}$$

The double integral in Eq. 54 was evaluated analytically for all integration shapes where possible, using the MATLAB symbolic integration functionality. In cases where the analytical procedure was not possible, the function *vpaintegral* (MathWorks, 2022) was used; this function has an adjustable relative error parameter that was set to 10^{-9}. Essentially, this procedure evaluates the integral numerically using a large number of integrand evaluations (up to 10^5) until the relevant error tolerance is met. By comparing the output of the 3-point Gauss quadrature, 2-point Gauss quadrature and 1-point evaluation with the results of exact integration, the error of the numerical integration of the kernels can be evaluated.

The results are shown in Fig. 17. As expected, the greater the number of intervals used, the smaller the resultant sub-partitioned integration shapes, and the lower the error. Furthermore, the error reduces with the use of more accurate integration rules. However, even with the 1-point integration scheme, which was employed in previous works such as Liu and Rigopoulos (2019), 40 intervals are sufficient to make the error less than 1%. With 3-point Gaussian quadrature, the numerical integration is

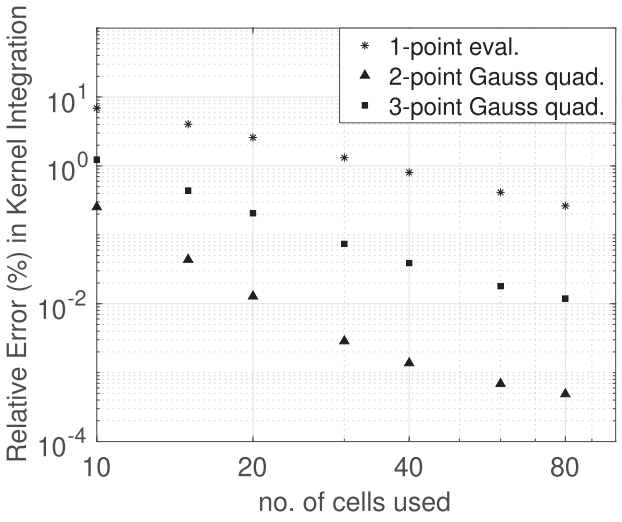

(a) Free-molecule kernel integration relative error (%)

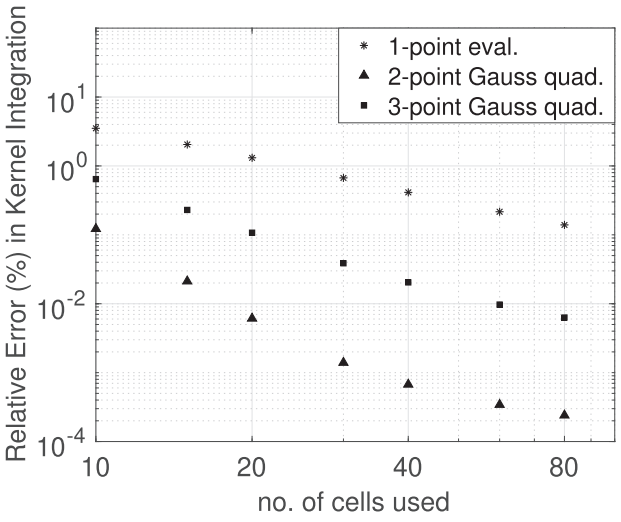

(b) Brownian kernel integration relative error (%)

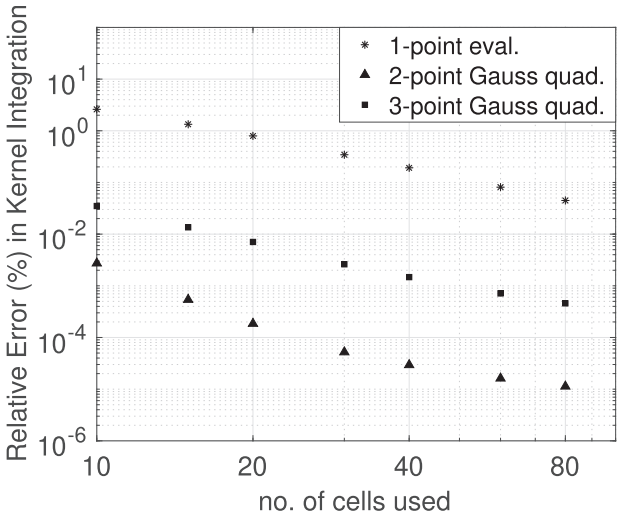

(c) Shear kernel integration relative error (%)

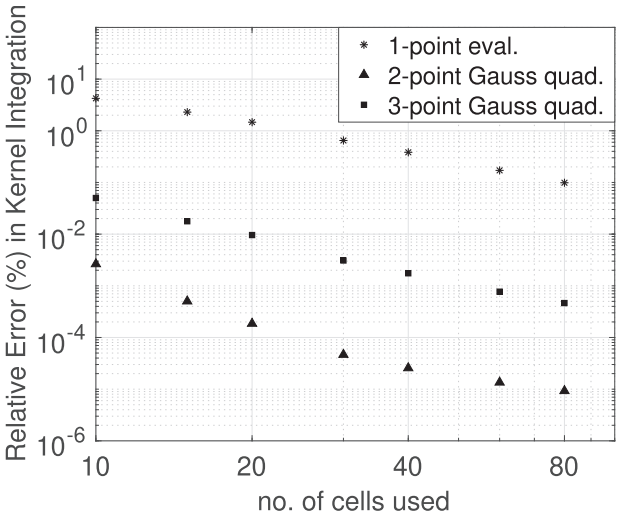

(d) Gravitational kernel integration relative error (%)

Fig. 17. Kernel integration relative errors (%) for the most important non-linear aggregation kernels.

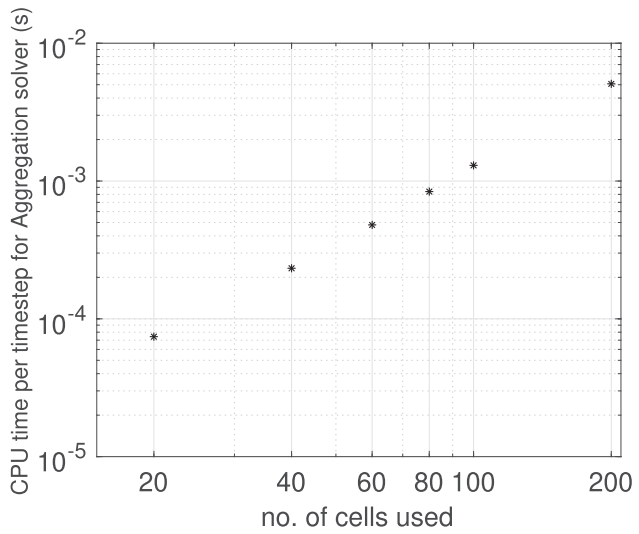

Fig. 18. CPU time taken per time-step to evaluate time-integration of aggregation routine in a pure aggregation case.

close to the exact result as an error less than 0.3 % is found across all kernels with as few as 10 intervals. It can be concluded that the error involved in the integration of the non-linear kernels is very small, and easily controlled. It should be emphasised that this is the only error involved in the treatment of the aggregation integral terms in the proposed method. This does not include, of course, the error associated with the discrete representation of the distribution, which is present in every discretisation method and can only be reduced by using a finer grid or a higher order approximation of the distribution itself within each interval.

5.9. Note on computational performance

The validation of the method has been carried out against solutions of the homogeneous PBE. With respect to the computational performance, it must first be acknowledged that any discretisation method would be very fast on modern computers when it comes to solving a single homogeneous PBE. However, efficiency becomes important if the method is to be coupled with CFD or used for optimisation where a very large number of PBEs must be solved.

In order to demonstrate the feasibility in the context of a larger CFD problem, it is important to take into account the parallel architecture typically employed for such simulations. A large CFD grid with millions of cells will have its domain split into many sub-domains, each of which will be sent to an individual CPU. This gives rise to a need to communicate results at each sub-domain boundary in order to evaluate the convection–diffusion step. Crucially, as a rule of thumb, an order of 10^4 CFD cells are assigned per processor. As with all parallel computing tasks, there is a trade-off between parallelisation and communication overhead. The PBE, alongside chemical reactions, is evaluated as part of the source term in a CFD solver. The source term is typically evaluated after the convection–diffusion step, and its output is required for the next convection–diffusion step to begin. If the number of CFD cells used *per processor* is considerably more than 10^4, the source term will take too long to evaluate, thus defeating the purpose of splitting the domain in the first place. On the contrary, if too few CFD cells are used per processor, then the reaction step may take too short a time relative to the communication overhead.

Based on the above, we can set a rough target for the duration of an individual PBE integration to be of the order 10^{-4} s. When scaled for 10^4 CFD cells, this yields approximately 1 s (i.e. 10^{-4} x 10^4) for the source term evaluation in the entire domain, which should be viable in the context of a larger CFD program. Fig. 18 shows that for grids of 80 intervals or less, this time step criterion is met. Furthermore, with the use of pre-tabulation of the relevant aggregation integrals, the CPU time per time step is independent of the choice of aggregation or fragmentation kernel.

It is also worth noting that the aggregation-growth part of the method in the Liu and Rigopoulos implementation (Liu and Rigopoulos, 2019) has been employed in coupled CFD-PBE simulations of soot formation in laminar flames (Liu and Rigopoulos, 2019; Liu et al., 2020; Sun et al., 2021) as well as in a DNS-PBE simulation of turbulent coagulation (Tsagkaridis et al., 2022). In Liu and Rigopoulos (2019), a detailed breakdown of CPU time was reported and the time taken by the PBE solver was 8.2% of the time taken by the whole simulation over an average over 200 time steps. The extension to fragmentation in the present paper requires fewer operations per time step than aggregation, while the use of Gaussian quadrature is carried out in the pre-tabulation step. These facts indicate that the computational demands of the method are modest and allow for its integration within CFD codes.

6. Conclusions

In the present work, a comprehensive approach for solving the PBE in problems featuring any combination of the population balance kinetic processes, namely aggregation, fragmentation, nucleation and growth was presented. The approach is based on the finite volume method, and emphasises conservation of the first moment - which is proportional to mass. The major source of conservation error was identified to be the aggregation birth term, whose convolution-like form prevents identifying the intervals from which the parent particles originate. A coordinate transformation was used to delineate the contributions to the aggregation birth term, and relate them to the appropriate death fluxes. An aggregation and a fragmentation map were constructed, which illustrate graphically how mass fluxes are assigned across the domain. Furthermore, the aggregation and fragmentation maps define the regions of integration resulting from the double integrals that arise from the application of the finite volume method to the integral terms in the PBE. The essence of the method is to partition the aggregation birth double integral in such a way, using the aggregation map, that its evaluation is exact apart from the kernel - for which numerical integration has to be employed. It was also shown that the non-linear kernels corresponding to physical processes can be integrated with high accuracy, thus practically eliminating the integration error. The method is conservative with respect to the first moment because it operates with fluxes, such that any outflow of parent particles results in a corresponding inflow at another part of the domain. It was also shown how the method can be combined with a TVD scheme in order to minimise numerical diffusion in problems including growth; an additional source term results in a mass-based TVD formulation and it was demonstrated that when accounting for, the first moment is predicted exactly in aggregation-growth problems.

The method was validated with a number of reference solutions for aggregation, fragmentation, aggregation-fragmentation and aggregation-growth. In all cases, the method was able to yield very accurate solutions for both the particle size distribution and moments, with a relatively small number of nodes. Another feature of the method is the ability to use an arbitrary grid, which makes it suitable for combining with adaptive grid methods such as the one presented in Sewerin and Rigopoulos (2017a). The implementation of the method is also computationally efficient, owing to the pre-tabulation of the aggregation and fragmentation maps. The operations that need to be performed at every time step are thus, very

few and straightforward. This feature renders the method suitable for problems where the PBE has to be coupled with CFD, and elements of the method (the aggregation approach in particular) have already been coupled successfully with CFD programs.

Future work will demonstrate the efficiency of the method in problems that feature complex combinations of transport and kinetic processes. The potential for accurate and conservative predictions will also be crucial for minimising numerical errors when comparing simulations with experiments. This will significantly aid in the identification of errors due to other sources such as: the flow field, the physical or chemical modelling itself and experimental uncertainties.

Declaration of Competing Interest

The authors declare that they have no known competing financial interests or personal relationships that could have appeared to influence the work reported in this paper.

Acknowledgements

Daniel O'Sullivan gratefully acknowledges financial support from the Engineering and Physical Sciences Research Council (EPSRC) in the form of a Doctoral Training Partnership (DTP). Stelios Rigopoulos gratefully acknowledges financial support from the Leverhulme Trust (grant RPG-2018–101). The authors are also grateful to Dr. Fabian Sewerin for suggesting the criterion of CPU time evaluation and for feedback on an early version of the paper.

Appendix A: Shapes in the aggregation map

In order to find and identify all the relevant shapes in the aggregation map in the context of an arbitrary grid, all possible relative sizes between parents cells (namely expanding, uniform and contracting) will have to be considered systematically. As outlined in the main body of the paper, the auxiliary grid is a function of both the daughter interval, and one of the parent intervals - thus: $U_k(\Delta v_i, \Delta w_j)$. Therefore, in order to examine the possible shapes and permutations, it is necessary to begin with the 3 basic cases that arise when comparing Δv_i and Δw_j in a given interval.

- Expanding interval: $\Delta v_i > \Delta w_j$
  - Calculate auxiliary grid, $U_k(\Delta v_i, \Delta w_j)$:
  - $U_1 = v_{i-1} - w_j; U_2 = v_{i-1} - w_{j-1}; U_3 = v_i - w_j; U_4 = v_i - w_{j-1}$;
  - Some key relations: $U_3 - U_1 = \Delta v_i$; $U_4 - U_2 = \Delta v_i$; $U_3 - U_2 = \Delta v_i - \Delta w_j$;
  - Since $\Delta v_i > \Delta w_j \rightarrow U_3 > U_2$
  - 3 classes of shapes appear: a *left-side triangle*, a *rectangular middle section* and a *right-side triangle*. Note how the auxiliary grid aligns with the boundaries of each shape (Fig. 3).
  - As the auxiliary grid does not, in general, align with the grid, the next step is to locate any grid boundaries that divide the exiting shapes into smaller ones. This allows for the product of number densities in the integral to be taken out of the integral, as they are constant, and leads to each subsequent shape existing in a region of constant number density pairs. For clarity, the integrand remains the same in each one of the following integrals and will be denoted $h(u, w\prime) = (u + w\prime)\beta(u, w\prime)$
  - Integrals for *whole shapes*, before checking for sub-partitioning:
    - Left-side triangle: $I = \int_{w_{j-1}}^{w_j} \int_{u=v_{i-1}-w}^{U_2} h(u, w\prime) du dw\prime$
    - Rectangular region: $I = \int_{w_{j-1}}^{w_j} \int_{U_2}^{U_3} h(u, w\prime) du dw\prime$
    - Right-side triangle: $I = \int_{w_{j-1}}^{w_j} \int_{U_3}^{u=v_i-w} h(u, w\prime) du dw\prime$
  - Integrals for *generalised shapes*, to account for sub-partitions:
    - Let $w_{LB} < w < w_{UB}$ and $u_{LB} < u < u_{UB}$define the sub-region.
    - Left-side triangles: $I = \int_{w_{LB}}^{w_{UB}} \int_{u=v_{LB}-w}^{u_{UB}} h(u, w\prime) du dw\prime$where $v_{LB} = w_{UB} - u_{LB}$
    - Rectangular region: $I = \int_{w_{LB}}^{w_{UB}} \int_{u_{LB}}^{u_{UB}} h(u, w\prime) du dw\prime$
    - Right-side triangle: $I = \int_{w_{LB}}^{w_{UB}} \int_{u_{LB}}^{u=v_{UB}-w} h(u, w\prime) du dw\prime$ where $v_{LB} = w_{UB} - u_{LB}$

- Uniform interval: $\Delta v_i = \Delta w_j$
  - Calculate auxiliary grid, $U_k(\Delta v_i, \Delta w_j)$:
  - $U_1 = v_{i-1} - w_j; U_2 = v_{i-1} - w_{j-1}; U_3 = v_i - w_j; U_4 = v_i - w_{j-1}$;
  - Some key relations: $U_3 - U_1 = \Delta v_i$; $U_4 - U_2 = \Delta v_i$; $U_3 - U_2 = 0$;
  - Since $\Delta v_i = \Delta w_j \rightarrow U_3 = U_2$. Thus, the central rectangular region found in the expanding case collapses and just two triangular regions are left to be evaluated.
    - Left-side triangle: $I = \int_{w_{j-1}}^{w_j} \int_{u=v_{i-1}-w}^{U_2} h(u, w\prime) du dw\prime$
    - Right-side triangle: $I = \int_{w_{j-1}}^{w_j} \int_{U_3}^{u=v_i-w} h(u, w\prime) du dw\prime$

- Contracting interval: $\Delta v_i < \Delta w_j$
  - Calculate auxiliary grid, $U_k(\Delta v_i, \Delta w_j)$:
  - $U_1 = v_{i-1} - w_j; U_2 = v_{i-1} - w_{j-1}; U_3 = v_i - w_j; U_4 = v_i - w_{j-1}$;
  - Some key relations: $U_3 - U_1 = \Delta v_i$; $U_4 - U_2 = \Delta v_i$; $U_3 - U_2 = \Delta v_i - \Delta w_j$;
  - Since $\Delta v_i < \Delta w_j \rightarrow U_3 < U_2$. Thus, U_3 is now to left of U_2 by definition and the remaining overall shape can be viewed as a left-side triangle, a right-side triangle and a parallelogram in between, Fig. 19.
    - Left-side triangle: $I = \int_{w_{j-1}}^{w_j} \int_{u=v_{i-1}-w}^{U_2} h(u, w\prime) du dw\prime$
    - Parallelogram: $I = \int_{U_3}^{U_2} \int_{w=v_{i-1}-u}^{w=v_i-u} h(u, w\prime) du dw\prime$
    - Right-side triangle: $I = \int_{w_{j-1}}^{w_j} \int_{U_3}^{u=v_i-w} h(u, w\prime) du dw\prime$

Appendix B: Integration of the kernel with Gaussian quadrature

In essence, the integral is transformed with a change of variables such that the integral now exists over a square ranging from -1 to 1 in the transformed space coordinates. This is straightforward for the rectangular integration shapes within the aggregation map, while the triangular regions will be treated below. Subsequently, the integrand is evaluated at the *Gauss points* and weighted by the appropriate *Gauss weights* (Heath, 2002). In the case of 2D 3-point Gauss quadrature, the integrand is sampled 9

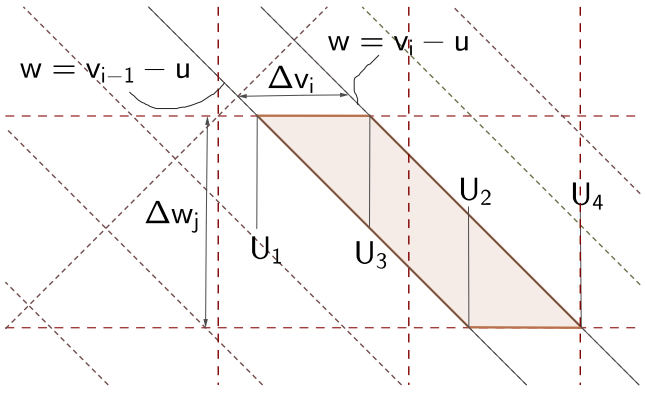

Fig. 19. Example of an interval on a contracting grid, used to highlight the left triangle, right triangle as well as the new parallelogram shape found in the region of integration.

times at the appropriate Gauss points within each sub-region of integration, S_p. Such a scheme can integrate polynomials of order $2 \times 3 - 1 = 5$ exactly.

Applying the Gaussian quadrature scheme to the triangular regions requires more attention, due to the variable integration limit representing a linear relationship between u and w i.e. $w = v_i - u$. The first step is to transform the inner integral to the domain [-1,1] with a change of variables. The general case for an arbitrary function is shown below:

$$\int_a^b f(x)dx = \int_{-1}^{1} f(\eta)\frac{b-a}{2}d\eta \tag{55}$$

where

$$x = \frac{b-a}{2}\eta + \frac{a+b}{2} \tag{56}$$

However, when this procedure is applied to the inner integral from Eq. 11, the lower limit is now in terms of $w\prime$, and this carries into the transformation itself. Let $g(u, w\prime)$ represent either integrand from Eq. 11. Thus:

$$\int_{u=v_{i-1}-w\prime}^{U_2} g(u,w')du \rightarrow \int_{-1}^{1} g(\eta,w')\frac{U_2-(v_{i-1}-w')}{2}d\eta \tag{57}$$

using:

$$u = \frac{U_2-(v_{i-1}-w')}{2}\eta + \frac{U_2+(v_{i-1}-w')}{2} \tag{58}$$

The transformed integral in Eq. 57 is now approximated using the Gaussian quadrature rules leading to the sum of the products of the necessary weights and integrand evaluations at the Gauss points (a_n and η_n, respectively).

$$\int_{-1}^{1} g(\eta,w')\frac{U_2-(v_{i-1}-w')}{2}d\eta \approx \sum_{n=1}^{NQP} a_n g(\eta_n,w')\frac{U_2-(v_{i-1}-w')}{2} \tag{59}$$

Now, the remaining sum is only a function of $w\prime$ and the procedure is repeated for the outer integral in Eq. 11, with constant integration limits w_{j-1} to w_j. Thus:

$$\approx \sum_{m=1}^{NQP}\sum_{n=1}^{NQP} a_n b_n g(\eta_n,\zeta_m)Y(\zeta_m) \tag{60a}$$

$$\text{where}: Y(\zeta_m) \equiv \frac{U_2-(v_{i-1}-(\frac{w_j-w_{j-1}}{2}\zeta_m+\frac{w_j+w_{j-1}}{2}))}{2}\frac{w_j-w_{j-1}}{2} \tag{60b}$$

Note that the transformation for $w\prime$ appears not only as an independent variable of $g(\eta_n, \zeta_m)$ but also in the ratio that immediately follows. This is due to the originally triangular region being transformed into a standardised square domain then approximated. For 2D 3-point Gaussian quadrature, $NQP = 3$, and the weights can be found in standard references such as Abramowitz and Stegun (1965).

Appendix C: Analytical solution for aggregation-breakage

The Patil-Andrews-Lage solution (Patil and Andrews, 1998; Lage, 2002) takes form as the results of an inverse-Laplacian operation and is shown in non-dimensional terms below:

$$\psi(\eta) = \sum_{i=1}^{2}\frac{K_1(\tau)+p_iK_2(\tau)}{L_2(\tau)+4p_i}\exp(p_i\eta) \tag{61}$$

where the non-dimensionalisation is done as follows:

$$\psi(\eta) = \frac{n(v,t)\phi}{N_0^2} \tag{62a}$$

$$\eta = \frac{vN_0}{\phi} \tag{62b}$$

$$\tau = N_0Ct \tag{62c}$$

Furthermore, a key criterion of this particular result is the balancing of coagulation and breakage rates such that Eq. 63 is satisfied. Note C is the coagulation kernel, S is the breakage rate, ϕ is the first moment in-terms of particle volume and N_0 is the initial total number density.

$$\sqrt{\frac{2S\phi}{C}} = N_0 \tag{63}$$

and the factors in Eq. 61 are defined below:

$$K_1(\tau) = 7 + \tau + e^{-\tau} \tag{64a}$$

$$K_2(\tau) = 2 - 2e^{-\tau} \tag{64b}$$

$$L_2(\tau) = 9 + \tau - e^{-\tau} \tag{64c}$$

$$p_{1,2} = \frac{1}{4}(e^{-\tau} - \tau - 9) \pm \frac{1}{4}\sqrt{d(\tau)} \tag{64d}$$

$$d(\tau) = \tau^2 + (10 - 2e^{-\tau})\tau + 25 - 26e^{-\tau} + e^{-2\tau} \tag{64e}$$

In the test case used, the breakage rate S, was set to 2 and the aggregation rate C, was set to 1. The steady total number density is thus found as follows (note that ϕ = 1 throughout):

$$N_0(t \rightarrow \infty) = \sqrt{\frac{2S\phi}{C}} \tag{65}$$

or $N_0(t \rightarrow \infty) = 2$.

References

Abramowitz, M., Stegun, I.A. (Eds.), 1965. Handbook of Mathematical Functions: with Formulas, Graphs, and Mathematical Tables. Dover Publications Inc, New York.

Batterham, R.J., Hall, J.S., Barton, G., 1981. Pelletizing kinetics and simulation of full scale balling circuits. In: 3rd International Symposium on Agglomeration, pp. A136–A150.

Bleck, R., 1970. A fast, approximative method for integrating the stochastic coalescence equation. J. Geophys. Res. 75, 5165–5171.

Bouaniche, A., Vervisch, L., Domingo, P., 2019. A hybrid stochastic/fixed-sectional method for solving the population balance equation. Chem. Eng. Sci. 209, 115198.

Campos, F.B., Lage, P.L.C., 2003. A numerical method for solving the transient multidimensional population balance equation using an Euler-Lagrange formulation. Chem. Eng. Sci. 58, 2725–2744.

Drake, R., 1972. A general mathematical survey of the coagulation equation. In: Hidy, G.M., Brock, J.R. (Eds.), Topics in Current Aerosol Research (Part 2). Pergamon Press, pp. 201–376.

Filbet, F., Laurençot, P., 2004. Numerical simulation of the Smoluchowski coagulation equation. SIAM Journal on Scientific Computing 25, 2004–2028.

Friedlander, S.K., 2000. Smoke, Dust, and Haze: Fundamentals of Aerosol Dynamics. 2nd ed., Oxford University Press.

Friedlander, S.K., Wang, C.S., 1966. The self-preserving particle size distribution for coagulation by Brownian motion. J. Colloid Interface Sci. 22, 126–132.

Gelbard, F., Seinfeld, J.H., 1978. Numerical solution of the dynamic equation for particulate systems. J. Comput. Phys. 28, 357–375.

Gelbard, F., Seinfeld, J.H., 1980. Simulation of multicomponent aerosol dynamics. J. Colloid Interface Sci. 78, 485–501.

Gelbard, F., Tambour, Y., Seinfeld, J.H., 1980. Sectional representations for simulating aerosol dynamics. J. Colloid Interface Sci. 76, 541–556.

Heath, M.T., 2002. Scientific computing: An introductory survey. McGraw-Hill.

Hill, P.J., Ng, K.M., 1995. New discretization procedure for the breakage equation. AIChE J. 41, 1204–1216.

Hill, P.J., Ng, K.M., 1996. New discretization procedure for the agglomeration equation. AIChE J. 42, 727–741.

Hounslow, M.J., 1998. The population balance as a tool for understanding particle rate processes. KONA Powder and Particle Journal 16, 179–193.

Hounslow, M.J., Ryall, R.L., Marshall, V.R., 1988. A discretized population balance for nucleation, growth, and aggregation. AIChE J. 34, 1821–1832.

Hulburt, H.M., Katz, S., 1964. Some problems in particle technology. A statistical mechanical formulation. Chem. Eng. Sci. 19, 555–574.

Jacobson, M.Z., 1997. Development and application of a new air pollution modeling system - II. Aerosol module structure and design. Atmos. Environ. 31, 131–144.
Koren, B., 1993. A robust upwind discretization method for advection, diffusion and source terms, in: Vreugdenhil, C.B., Koren, B. (Eds.), Numerical Methods for Advection-Diffusion Problems. Vieweg Verlag. volume 45 of Notes on Numerical Fluid Mechanics and Multidisciplinary Design, pp. 117–138.
Kostoglou, M., 2007. Extended cell average technique for the solution of coagulation equation. J. Colloid Interface Sci. 306, 72–81.
Kostoglou, M., 2007. The linear breakage equation: From fundamental issues to numerical solution techniques. In: Williams, J.C., Allen, T., Salman, A.D., Ghadiri, M., Hounslow, M.J. (Eds.), Handbook of Powder Technology, Volume 12: Particle Breakage. Elsevier, pp. 793–835.
Kostoglou, M., Karabelas, A.J., 1994. Evaluation of zero order methods for simulating particle coagulation. J. Colloid Interface Sci. 163, 420–431.
Kumar, J., Peglow, M., Warnecke, G., Heinrich, S., Mörl, L., 2006. Improved accuracy and convergence of discretized population balance for aggregation: The cell average technique. Chem. Eng. Sci. 61, 3327–3342.
Kumar, J., Peglow, M., Warnecke, G., Heinrich, S., Tsotsas, E., Mörl, L., Hounslow, M., Reynolds, G., 2007. Numerical methods on population balances. In: Tsotsas, E., Mujumdar, A.S. (Eds.), Modern Drying Technology. Wiley-VCH Verlag GmbH & Co. KGaA, pp. 209–260.
Kumar, J., Saha, J., Tsotsas, E., 2015. Development and convergence analysis of a finite volume scheme for solving breakage equation. SIAM Journal on Numerical Analysis 53, 1672–1689.
Kumar, S., Ramkrishna, D., 1996a. On the solution of population balance equations by discretization - I. A fixed pivot technique. Chem. Eng. Sci. 51, 1311–1332.
Kumar, S., Ramkrishna, D., 1996b. On the solution of population balance equations by discretization - II. A moving pivot technique. Chem. Eng. Sci. 51, 1333–1342.
Kumar, S., Ramkrishna, D., 1997. On the solution of population balance equations by discretization - III. Nucleation, growth and aggregation of particles. Chem. Eng. Sci. 52, 4659–4679.
Lage, P.L.C., 2002. Comments on the "An analytical solution to the population balance equation with coalescence and breakage - the special case with constant number of particles" by D.P. Patil and J.R.G. Andrews [Chemical Engineering Science 53(3), 599–601]. Chem. Eng. Sci. 57, 4253–4254.
Lai, F.S., Friedlander, S.K., Pich, J., Hidy, G.M., 1972. The self-preserving particle size distribution for Brownian coagulation in the free-molecule regime. Journal of Colloid And Interface Science 39, 395–405.
Landgrebe, J.D., Pratsinis, S.E., 1989. Gas-phase manufacture of particulates: Interplay of chemical reaction and aerosol coagulation in the free-molecular regime. Ind. Eng. Chem. Res. 28, 1474–1481.
Landgrebe, J.D., Pratsinis, S.E., 1990. A discrete-sectional model for particulate production by gas-phase chemical reaction and aerosol coagulation in the free-molecular regime. J. Colloid Interface Sci. 139, 63–86.
Laurent, F., Sibra, A., Doisneau, F., 2016. Two-size moment multi-fluid model: A robust and high-fidelity description of polydisperse moderately dense evaporating sprays. Communications in Computational Physics 20, 902–943.
Litster, J.D., Smit, D.J., Hounslow, M.J., 1995. Adjustable discretized population balance for growth and aggregation. AIChE J. 41, 591–603.
Liu, A., Garcia, C.E., Sewerin, F., Williams, B.A.O., Rigopoulos, S., 2020. Population balance modelling and laser diagnostic validation of soot particle evolution in laminar ethylene diffusion flames. Combust. Flame 221, 384–400.
Liu, A., Rigopoulos, S., 2019. A conservative method for numerical solution of the population balance equation, and application to soot formation. Combust. Flame 205, 506–521.
Ma, D.L., Tafti, D.K., Braatz, R.D., 2002. High-resolution simulation of multidimensional crystal growth. Ind. Eng. Chem. Res. 41, 6217–6223.
MathWorks, 2022. MATLAB documentation. URL: https://www.mathworks.com/help/releases/R2021a/symbolic/vpaintegral.html?s_tid=doc_srchtitle. Accessed: 10/07/2022.
Nguyen, T.T., Laurent, F., Fox, R.O., Massot, M., 2016. Solution of population balance equations in applications with fine particles: Mathematical modeling and numerical schemes. J. Comput. Phys. 325, 129–156.
Nicmanis, M., Hounslow, M.J., 1998. Finite-element methods for steady-state population balance equations. AIChE J. 44, 2258–2272.
Patil, D.P., Andrews, J.R.G., 1998. An analytical solution to continuous population balance model describing floc coalescence and breakage - A special case. Chem. Eng. Sci. 53, 599–601.
Qamar, S., Elsner, M.P., Angelov, I.A., Warnecke, G., Seidel-Morgenstern, A., 2006. A comparative study of high resolution schemes for solving population balances in crystallization. Comput. Chem. Eng. 30, 1119–1131.
Qamar, S., Warnecke, G., Elsner, M.P., 2009. On the solution of population balances for nucleation, growth, aggregation and breakage processes. Chem. Eng. Sci. 64, 2088–2095.
Ramabhadran, T.E., Peterson, T.W., Seinfeld, J.H., 1976. Dynamics of aerosol coagulation and condensation. AIChE J. 22, 840–851.
Raman, V., Fox, R.O., 2016. Modeling of fine-particle formation in turbulent flames. Annu. Rev. Fluid Mech. 48, 159–190.
Ramkrishna, D., 1985. The status of population balances. Rev. Chem. Eng. 3, 49–95.
Ramkrishna, D., 2000. Population Balances: Theory and Applications to Particulate Systems in Engineering. Academic Press.
Ramkrishna, D., Mahoney, A.W., 2002. Population balance modeling. promise for the future. Chem. Eng. Sci. 57, 595–606.
Ramkrishna, D., Singh, M.R., 2014. Population balance modeling: Current status and future prospects. Annual Review of Chemical and Biomolecular Engineering 5, 123–146.
Rigopoulos, S., 2010. Population balance modelling of polydispersed particles in reactive flows. Prog. Energy Combust. Sci. 36, 412–443.
Rigopoulos, S., 2019. Modelling of soot aerosol dynamics in turbulent flow. Flow, Turbulence and Combustion 103, 565–604.
Rigopoulos, S., Jones, A., 2003. Finite-element scheme for solution of the dynamic population balance equation. AIChE J. 49, 1127–1139.
Roussos, A.I., Alexopoulos, A.H., Kiparissides, C., 2005. Part III: Dynamic evolution of the particle size distribution in batch and continuous particulate processes: A Galerkin on finite elements approach. Chem. Eng. Sci. 60, 6998–7010.
Schumann, T.E.W., 1940. Theoretical aspects of the size distribution of fog particles. Quarterly Journal of the Royal Meteorological Society 66, 195–208.
Scott, W.T., 1968. Analytic studies of cloud droplet coalescence i. Journal of the Atmospheric Sciences 25, 54–65.
Sewerin, F., 2022. A methodology for solving the population balance equation based on an embedded reduced order representation. Chem. Eng. Sci. 252, 117101.
Sewerin, F., Rigopoulos, S., 2017a. An explicit adaptive grid approach for the numerical solution of the population balance equation. Chem. Eng. Sci. 168, 250–270.
Sewerin, F., Rigopoulos, S., 2017b. An LES-PBE-PDF approach for modeling particle formation in turbulent reacting flows. Phys. Fluids 29, 105105.
Sewerin, F., Rigopoulos, S., 2018. An LES-PBE-PDF approach for predicting the soot particle size distribution in turbulent flames. Combust. Flame 189, 62–76.
Shiea, M., Buffo, A., Vanni, M., Marchisio, D., 2020. Numerical methods for the solution of population balance equations coupled with computational fluid dynamics. Annual Review of Chemical and Biomolecular Engineering 11, 339–366.
Singh, M., Walker, G., 2022. Finite volume approach for fragmentation equation and its mathematical analysis. Numerical Algorithms 89, 465–486.
Smoluchowski, M.v., 1917. Versuch einer mathematischen Theorie der Koagulationskinetik kolloider Lösungen. Zeitschrift für Physikalische Chemie 92, 129–168.
Solsvik, J., Jakobsen, H.A., 2015. The foundation of the population balance equation: A review. J. Dispersion Sci. Technol. 36, 510–520.
Spielman, L.A., Levenspiel, O., 1965. A Monte Carlo treatment for reacting and coalescing dispersed phase systems. Chem. Eng. Sci. 20, 247–254.
Spivak, M., 1994. Calculus. Cambridge University Press.
Sporleder, F., Borka, Z., Solsvik, J., Jakobsen, H.A., 2012. On the population balance equation. Rev. Chem. Eng. 28, 149–169.
Sun, B., Rigopoulos, S., Liu, A., 2021. Modelling of soot coalescence and aggregation with a two-population balance equation model and a conservative finite volume method. Combust. Flame 229, 111382.
Swift, D.L., Friedlander, S.K., 1964. The coagulation of hydrosols by Brownian motion and laminar shear flow. J. Colloid Sci. 19, 621–647.
Thompson, P.D., 1968. A transformation of the stochastic equation for droplet coalescence, in. In: Proceedings of the International Conference on Cloud Physics, pp. 115–126.
Tsagkaridis, M., Rigopoulos, S., Papadakis, G., 2022. Analysis of turbulent coagulation in a jet with discretised population balance and DNS. J. Fluid Mech. 937, A25.
Tsang, T.H., Brock, J.R., 1982. Simulation of condensation aerosol growth by condensation and evaporation. Aerosol Sci. Technol. 2, 311–320.
Vanni, M., 2000. Approximate population balance equations for aggregation-breakage processes. J. Colloid Interface Sci. 221, 143–160.
Williams, M.M.R., Loyalka, S.K., 1991. Aerosol Science - Theory and Practice: With Special Applications to the Nuclear Industry. Pergamon Press, Oxford.
Yang, S., Mueller, M.E., 2019. A Multi-Moment Sectional Method (MMSM) for tracking the soot Number Density Function. Proc. Combust. Inst. 37, 1041–1048.
Ziff, R.M., 1991. New solutions to the fragmentation equation. J. Phys. A: Gen. Phys. 24, 2821–2828.
Ziff, R.M., McGrady, E.D., 1985. The kinetics of cluster fragmentation and depolymerisation. J. Phys. A: Math. Gen. 18, 3027–3037.